

1 **Controls on the surface expression of growth faults in volcanic rift zones**

2 **A. Bubeck¹, R.J. Walker¹, J. Imber², C.J. MacLeod³**

3 ¹*Department of Geology, University of Leicester, University Road, Leicester, UK.*

4 ²*Department of Earth Sciences, Durham University, Science Labs, Durham, UK.*

5 ³*School of Earth and Ocean Science, Cardiff University, Park Place, Cardiff, UK*

6 *Correspondence (ab753@le.ac.uk)

7

8 **ABSTRACT**

9 Conceptual models for the evolution of dilatant faults in volcanic rift settings involve a step-wise
10 growth pattern, involving upward propagation of subsurface faults, surface monocline formation,
11 which are breached by subvertical, open faults. Immature, discontinuous normal faults are
12 considered representative of the early stages of mature, linked faults that accommodate extensional
13 strains. We consider the evolution of surface-breaching normal faults using a comparison of the
14 distribution and geometry of normal faults from two volcanic rift zones: the Koa'e fault system,
15 Hawai'i, and the Krafla fissure swarm, NE Iceland. Field mapping highlights similarities to current
16 predicted geometries, but also prominent differences that are not reconciled by current models.
17 Variable deformation styles record magma supply changes within the rift zones, which drive local
18 strain rate gradients. Building on existing studies, we present a conceptual model of fault growth
19 that accounts for spatial and temporal changes in strain rate within the deforming regions. We
20 propose that faults in separate rift systems may not advance through the same stages of evolution
21 and that faults within *individual* rift systems can show differing growth patterns. Variations in
22 surface strains may be indicative of subsurface magmatic system changes, with important
23 implications for our understanding of volcano-tectonic coupling.

24
25
26

Key words: normal fault; monocline; extension; basalt; volcanic rift

27 **1.1. Introduction**

28 Normal fault systems comprise discontinuous, non-collinear segments, with overlaps and segment
29 linkage forming characteristic en echelon geometries across a broad range of scales (e.g. Segall
30 and Pollard, 1980; Peacock, 2002; Long and Imber, 2011). Regional extension is conserved ahead
31 of first-order fault terminations by areas of folding and linking faults and fractures (e.g. Morley et
32 al., 1990; Faulds and Varga, 1998). The geometry and distribution of structures within these
33 domains play an important role in the tectono-stratigraphic development of rift basins (e.g.
34 Lambiase and Bosworth, 1995; Sharp et al., 2000; Hus et al., 2006), and the evolving fluid flow
35 properties of fault zones (e.g. Manzocchi et al., 2010; Seebeck et al., 2014). Much of our current
36 understanding of the growth of normal fault populations and fault zone architecture is derived from
37 studies of faults in clastic sequences using combinations of: (1) fault analysis and scaling
38 relationships based on field and seismic data-derived measurements of displacement and length
39 versus width (e.g. Ferrill and Morris, 2001; Peacock, 2002; Walsh et al., 2003; Nixon et al., 2014);
40 (2) scaled-analogue modelling (e.g. Holland et al., 2006; Tentler and Acocella, 2010); and (3)
41 numerical-based modelling techniques (e.g. Crider and Pollard, 1998; Maerten et al., 2002;
42 Schöpfer et al., 2006). Many of these studies have focussed on fault propagation and segmentation
43 within layered clastic sequences (e.g. Ferrill and Morris, 2003), and more recently crystalline-
44 clastic sequences (e.g. Peacock and Parfitt, 2002; Holland et al., 2006; Martel and Langley, 2006;
45 Kaven and Martel, 2007; Walker et al., 2013). The growth of normal faults in layered basaltic
46 sequences, and the expression of those faults outcropping at surface, has become increasingly
47 important in recent years, driven in part by the increasing economic viability of intra- and sub-

48 volcanic hydrocarbon plays along volcanic passive margins (e.g., the NE Atlantic basins: Davison
49 et al., 2004; Walker et al., 2012, 2013), as well as high-temperature shallow geothermal systems
50 that rely on basaltic stratigraphy (e.g. Anderson and Bowers, 1995; Helm-Clark et al., 2004) and
51 models of volcanic flank stability (e.g. Le Corvec and Walter, 2009; Plattner et al., 2013). An
52 improved understanding of basalt-hosted fault zones has important implications for extension in
53 continental and oceanic systems on Earth as well as on other planets.

54 Existing models for the growth of normal faults in basaltic sequences typically depict
55 development in a common series of static stages with the progression between stages inferred to
56 be instantaneous (e.g. Martel and Langley, 2006). Emphasis is placed on the reactivation of pre-
57 existing cooling joints through the entire layer sequence; considered to be the first-order control
58 on the distribution, geometry and architecture of basalt-hosted fault zones (e.g. Forslund and
59 Gudmundsson, 1992; Gudmundsson, 2011). A single evolutionary process implies that small-
60 displacement faults in immature or early-stage rift systems are also representative of faults in more
61 advanced systems, with all faults progressing through the same stages of evolution. As such,
62 models of fault growth in cohesive sequences are broadly applied to a wide range of settings.

63 Here, we present a detailed field study of the distribution and geometry of well-exposed
64 extensional structures in two developing volcanic rift zones - the Koa'e fault system, Hawai'i, and
65 the Krafla fissure swarm, NE Iceland - to compare and contrast evolving segmentation patterns
66 during rift development. Field mapping reveals that surface-breaching faults in separate rift
67 systems can follow different evolution pathways during propagation. Faults that are located within
68 *individual* rift systems can also demonstrate differing growth patterns. Our new observations build
69 on previous observations (e.g. Grant and Kattenhorn, 2004; Holland et al., 2006; Martel and

70 Langley, 2006; Kaven and Martel, 2007), and extend models, conceptually, for fault growth in
71 layered basaltic sequences.

72

73 **2.1. Background: near-surface faults in layered basaltic sequences**

74 Existing studies of near-surface normal fault development in layered basaltic sequences identify
75 four principal characteristics: (1) sinuous zones of vertical extension fractures (dominantly in the
76 footwall, but also in the hanging wall); (2) monoclinial flexure of the ground surface; (3) sub-
77 vertical, surface-breaking fault scarps that show a component of dilation; and (4) less commonly,
78 hanging wall buckles found proximally to the scarp bases (Duffield, 1975; Acocella et al., 2000;
79 Grant and Kattenhorn, 2004; Martel and Langley, 2006; Holland et al., 2006; Villemin and
80 Bergerat, 2013). These characteristics are expected to show predictable geometries, resulting from
81 the following successive stages: (1) nucleation of a normal fault at depth; (2) slip on the fault at
82 depth drives flexure of the free surface into a monocline, and cooling joints in the footwall ahead
83 of the fault tip begin to open; (3) with continued slip and upward propagation, the monocline
84 becomes steeper and narrower, and footwall fractures widen and propagate downwards; (4)
85 eventual linkage of surface extension fractures with fault tips at depth leads to systematic breaching
86 of surface monoclines and the development of sub-vertical, surface-breaking fault segments that
87 display horizontal and vertical components of displacement. Although previous work has invoked
88 a downward fault growth model (e.g. Opheim and Gudmundsson, 1989), here we focus on upward
89 propagation, which is best supported by field observations and numerical models (e.g. Grant and
90 Kattenhorn, 2004; Kaven and Martel, 2007). Numerical-based models of the evolution of tensile
91 and compressive stresses ahead of propagating normal faults have found that an upward
92 propagating model produces consistent distributions of footwall and hanging wall extension

93 fracture networks, and hanging wall (compressive) buckles as are recorded in field examples
94 (Martel and Langley, 2006; Kaven and Martel, 2007).

95 Based on these models, we might expect predicted geometries (i.e. monoclinical folding of
96 basaltic layering) to be preserved at depth following upward propagation (e.g. Holland et al.,
97 2006). Notably, field studies of exhumed basaltic fault zones have found little evidence for folding,
98 implying that they may not represent precursory features of all basalt-hosted normal faults (e.g.
99 Walker et al., 2012, 2013).

100 To date, an upward growth model has been broadly applied to normal fault growth in
101 cohesive sequences for a range of geological settings including the Koa‘e fault system, Hawai‘i
102 (e.g. Holland et al., 2006; Podolsky and Roberts, 2008), Iceland (e.g. Grant and Kattenhorn, 2004;
103 Villemin and Bergerat, 2013), the East Africa Rift (e.g. Casey et al., 2006; Rowland et al., 2007),
104 mid ocean ridges (e.g. Soule et al., 2009; Escartin et al., 2016), Mars (e.g. Tanaka et al., 2008),
105 and Earth’s Moon (e.g. Nahm and Schultz, 2015). Most of the models derived for these systems
106 involve a deforming volume that is mechanically isotropic, and undergoes uniformly applied
107 boundary stresses at a constant strain rate. Using detailed field observations of surface structures
108 in the Koa‘e fault system, Hawai‘i and the Krafla fissure swarm in northern Iceland, we build upon
109 the existing field-data-constrained numerical models of Martel and Langley (2006) and
110 demonstrate that there is an inherently four-dimensional distribution of extensional strains and
111 strain rates within developing volcanic rift zones. Our aim is to show that the evolving first-order
112 geometry and distribution of normal faults is sensitive to variations in boundary stress conditions
113 and the mechanical properties of the deforming sequence.

114

115 **2.2. Methods**

116 Surface structures in the Koa‘e and Krafla fault systems were mapped using a combination of high
117 resolution aerial images (GoogleEarth™ and World-View2: 0.5 m resolution), topographic
118 datasets (aerial LiDAR: 0.5 m resolution (Koa‘e only)), and traditional field mapping techniques.
119 At the free surface, in both study areas, extension fractures (hereafter, *fractures*) appear to have
120 initiated along pre-existing cooling joints in the lava pile, producing characteristic zigzag trace
121 geometries (Figure 1), as presented previously (e.g. Grant and Kattenhorn, 2004; Martel and
122 Langley, 2006; Villemin and Bergerat, 2013).

123

124 *FIGURE 1 HERE*

125

126 This zig-zag geometry presents multiple piercing points in plan view, allowing displaced walls to
127 be matched across the open fracture aperture, and hence accurate measurement of the following
128 (see Figure 1): (1) extension direction and mode (extension, mode-I; extensional-shear, mixed-
129 mode); (2) the amount of horizontal opening across the fracture, here referred to as fracture
130 aperture; (3) fracture trace azimuth, equivalent to the strike of the fault plane; and (4) vertical offset
131 of the free surface, where present. Remote and field data are used to characterise the distribution,
132 and geometry of fractures and surface-breaking normal faults, as well as monocline distribution,
133 extent, and geometry to sub-metre precision and accuracy.

134

135 **3. Surface-breaking fault systems in volcanic rift zones**

136 **3.1. Early stage rift development: The Koa‘e fault system, Hawai‘i**

137 The Koa‘e fault system borders the south flank of Kīlauea Volcano (Figure 2A), which is the
138 youngest and southernmost subaerial volcano in the Hawaiian-Emperor chain, and one of five

139 volcanic systems on the Island of Hawai‘i (Neal and Lockwood, 2003). Melting generated by an
140 upwelling mantle plume impinges on the lithosphere, through which magma ascends via a system
141 of conduits into a series of interconnected shallow storage reservoirs at ~2.5-4 km and at ~2 km
142 depth beneath Kīlauea’s summit (e.g. Baker and Amelung, 2012, Lin et al., 2014). Repeated influx
143 of magma into these storage reservoirs, at rates of $\sim 0.1 \text{ km}^3 \text{ y}^{-1}$ (Swanson et al., 1976; Dzurisin et
144 al., 1984; Poland et al., 2014), typically results in episodes of inflation and deflation, driving
145 eruptive episodes either at the summit, or shallow intrusion and eruption within two pronounced
146 rift zones: the Southwest and East Rift Zones (Figure 2), which radiate south-westward and
147 eastward from the summit (Duffield et al., 1982; Wright and Klein, 2006; Poland et al., 2012).
148 Records of sustained eruptions at Kīlauea’s summit show that the duration and volume of magma
149 associated with eruptive episodes can vary significantly: In June 1952, $38 \times 10^6 \text{ m}^3$ of magma was
150 erupted over 136 days and in November 1967, $64 \times 10^6 \text{ m}^3$ of magma was erupted over 251 days.
151 Between 1983-2003, Kīlauea was in a phase of continuous eruption with $\sim 200 \times 10^6 \text{ m}^3$ of magma
152 released (Dvorak and Dzurisin, 1993; Poland et al., 2012). As a result of complex dynamics of the
153 system, extension rates across Kīlauea also vary considerably from: $\sim 26 \text{ cm/y}^{-1}$ between 1975-
154 1983 to $< 5 \text{ cm/y}^{-1}$ since 1983 (Delaney et al., 1990, 1998). Flank displacement is linked to periods
155 of shallow intrusion within the rift zones and summit region, and/or periods of gravitational sliding
156 on a basal detachment at a depth of approximately 9 km (e.g. Klein et al., 1987; Delaney et al.,
157 1990; Denlinger and Okubo, 1995; Le Corvec and Walter, 2009).

158

159 *FIGURE 2 HERE*

160

161 Our study area is within the Koa‘e fault system, which is a 12 km long, ~3 km wide zone
162 of normal faulting (Figure 2A), that connects the Southwest and East Rift Zones (SWRZ and ERZ,
163 hereafter) to form a continuous, 60-70 km long, ENE-WSW trending zone of extension. Normal
164 faults in the system are growth faults, interpreted to be related both to the forceful emplacement
165 of dykes into the rift zones of Kīlauea Volcano (Duffield et al., 1975, 1982; Swanson et al 1976;
166 Peacock and Parfitt, 2002) and to gravitationally induced volcano spreading (Poland et al., 2014
167 and references therein).

168

169 **3.1.1. Surface structures in the Koa‘e fault system**

170 Mapping in the Koa‘e fault system reveals three characteristic structures (Figure 2B): (1) first-
171 order ERZ-parallel (ENE-WSW striking) faults, with sub-vertical NNW-dipping scarps that show
172 maximum throws of 12-15 m; (2) second-order fracture networks that form discontinuous zones;
173 and (3) N to NNW-dipping monoclinial folds, which are discontinuous, show variable amplitudes
174 of up to 12 m, and have crests that are parallel to the strike of first-order faults and the strike of the
175 ERZ. An additional feature located in the immediate hanging wall of some faults are localized
176 buckle structures with anticlinal crests that parallel the strike of the ERZ and show amplitudes of
177 up to 2 m. The second-order fracture networks can be grouped into two dominant orientations:
178 ENE-WSW (ERZ-parallel) and NW-SE (ERZ-oblique). NW-SE striking fracture sets are less
179 common and observed as obliquely oriented steps along fracture (cm-10s of m scale) and fault
180 (100s of m- km scale) traces (Bubeck et al. in review).

181 Second-order extension fractures are limited to discontinuous, sinuous zones up to ~5 km
182 in length and 30-50 m wide (Figure 3A). Most of these zones are limited to the footwalls of surface-
183 breaking normal faults and along the upper limb of monoclines, where they parallel the strike of

184 the fold crest (Figure 3A). Less commonly, they are found in the hanging walls of faults, and as
185 isolated zones in areas of the fault system where fault scarps are absent and there is no evidence
186 for monoclinial flexure of the surface (Figure 3B, C).

187

188 *FIGURE 3 HERE*

189

190 Zones of rift-parallel (ENE-WSW) fractures are most common (~85% of mapped traces) and show
191 individual fracture trace lengths of up to ~370 m. Apertures may be as much as ~4 m, but are more
192 commonly in the range of 0.3-0.6 m. NW-SE striking fracture zones are less common (~15% of
193 mapped traces) with individual fracture trace lengths of ~4-120 m and apertures of 0.02-2.50 m.

194 Field characterization of fractures in the study identified only extensional openings (i.e. orthogonal
195 to fracture azimuth; e.g. Figure 1) and we recorded no preferred stepping direction between
196 segmented fracture traces. NW-SE striking fractures tend to occur in close association with the
197 lateral terminations of first-order rift-parallel normal faults and footwall fractures, occurring as
198 obliquely oriented steps or linkages between segments (Figure 2B; Bubeck et al., in review).

199 Individual fractures that outcrop for >10 m (Figure 3B) in the study area commonly display
200 multiple steps along their length in plan view, suggesting they represent composite fractures
201 produced by linkage of segments (e.g. Peacock and Sanderson, 1991). At the scale of the individual
202 fractures (i.e. beyond the scale of joint-related irregularities), shorter fractures (<10 m in length)
203 also display non-linear traces with obliquely oriented steps, hook-shaped tips, or abutting
204 geometries in the vicinity of neighboring structures (Figure 3C). Fractures of this length scale are
205 most commonly found along the upper limbs of monoclines where they form distributed networks
206 (Figure 3A, 4A, 5A). In some instances, these fractures are closely associated with the maximum

207 curvature of the monocline limb, indicating that outer arc stretching may contribute to their
208 opening. Composite fracture traces, with apertures of up to 5 m tend to form localized features
209 (Figure 4B, 5B).

210 Monoclinial folds in the Koa'e fault system may be divided into two scales: (1) monoclines
211 that are laterally continuous at the kilometre scale, for distances up to 3 km (Figure 2B, 4A); and
212 (2) monoclines that are laterally discontinuous, with maximum lengths of ~150 m (Figure 4B, 5B).

213

214 *FIGURE 4 HERE*

215

216 Continuous monoclines are observed in the western and central-western areas of the fault system
217 (Figure 2B); limbs dip gently (up to $\sim 10^\circ$) (Figure 4A, 5A), and show rounded fold morphologies
218 with amplitudes of up to ~ 12 m (Figure 6). Continuous monocline width varies considerably along
219 the fault system with widths generally decreasing with increasing fracture localisation and fault
220 breaching (Figure 6).

221

222 *FIGURE 5 HERE*

223

224 This is in agreement with the models of Martel and Langley (2006) and Kaven and Martel (2007)
225 who predicted monoclines will steepen and become narrower as faults approach the free surface.
226 Such patterns were also recorded by Podolsky and Roberts (2008) along the White Rabbit Fault
227 (Figure 2b); these authors, however, instead linked along-strike variations in monocline amplitude
228 to local occurrence of relay ramps ahead of the tips of previously soft-linked segments, rather than
229 to upward propagation-related folding.

230

231 *FIGURE 6 HERE*

232

233 Such fault tip monoclines are particularly clear along the Ohale Pali (Figure 2B) where
234 discontinuous folds occur as isolated lenses caught between en echelon fault segments (Figure
235 5C). The monoclines described in this study, however, are distinct from this relay ramp tilting
236 mechanism.

237 Discontinuous monoclines are restricted to the eastern region of the Koa'e fault system,
238 and are most common along the Kulanaokuaiki Fault (Figure 2B) where they form isolated,
239 disintegrated blocks with maximum amplitudes of up to ~12 m in the centre of each block,
240 decreasing steeply (~30°) to zero at the lateral tips (Figure 4B, 5B). Breached examples were not
241 observed. The hanging wall free surface that is offset across adjacent fault scarps is relatively flat.
242 The width of the folded limb of these structures does not vary greatly, ranging from 10 to 20 m.
243 These monoclines feature large (often >4 m wide) composite fractures along their upper limb and
244 tend to be connected laterally with large, open fault scarps with vertical offsets up to 12 m.
245 Monoclines of this type are decoupled from the footwall along these continuous co-linear
246 composite extension fractures (Figure 4B, 5B, 7A). The limited lateral extent of the short
247 monoclines, fragmented appearance, and localised steep dip are consistent with a fault-bound
248 block rotation of the immediate hanging wall, effected by blind antithetic faults rather than a
249 monoclinal fold. Such rotational features have been produced in analogue models of fault
250 propagation in brittle sequences (e.g. Holland et al., 2006; Michie et al., 2014).

251 It is important to note that monoclines of either type are not ubiquitous features of the fault
252 system and, where present, neither type has been systematically breached, despite being parallel

253 to the strike of prominent normal faults in the region. Where breaching has been observed, vertical
254 offsets on the monocline-breaching segments are minor (1-2 m) compared to collinear fault scarps
255 (up to 12 m throw).

256

257 *FIGURE 7 HERE*

258

259 Where present, sub-vertical normal faults in the area typically offset the surface by up to
260 ~15 m (Figure 7). In addition to a vertical component of displacement, all surface-breaking fault
261 segments exhibit horizontal openings along composite fracture traces with apertures of up to ~5
262 m. Fault scarps preserve cooling joint-related irregularities (e.g. Figure 1) and we find no evidence
263 for slickenlines or slickensides on fracture surfaces to indicate initial shear displacement,
264 consistent with observations in previous studies (e.g. Holland et al., 2006; Peacock and Parfitt,
265 2002).

266 It is not possible to determine from field study alone whether fault slip at depth was purely
267 dip-slip. Seismicity records suggest that strike-slip and oblique-slip faulting is common at depths
268 of 0.5-5.0 km below the Koa'e fault system (Lin and Okubo, 2016), but the surface expression of
269 this on the mapped faults is unclear. Mapping has revealed that surface-breaking normal fault
270 segments (up to 200 m in length) are most commonly found in the central-eastern and eastern
271 regions of the fault system, within ~5 km of the upper ERZ. Based on the total lengths of
272 deformation zones (up to 5 km; Figure 2B), our interpretation of these segments is that they
273 represent discontinuous splays of single fault structures at depth. Based on remote mapping
274 techniques, surface-breaking fault segments that offset planar footwall and hanging wall surfaces
275 are estimated to comprise approximately 20% of fault traces in the Koa'e fault system; the

276 remaining ~80% is characterised by monoclinial folding, blind normal faults, and rarely,
277 monocline-breaching fault segments.

278

279 **3.2. Advanced stage rift development: The Krafla fissure swarm, Iceland**

280 Iceland is located on the plate boundary between North America and Eurasia, and represents a
281 subaerially exposed segment of the Mid-Atlantic Ridge. The Icelandic axial rift zone (the Neo-
282 Volcanic Zone: NVZ) accommodates WNW-ESE (104°) extension of ~19 mm/year (e.g.
283 Sæmundsson, 1974; Wright et al., 2012) across 5 sub-parallel NNE-SSW-striking en echelon
284 volcanic systems and associated fissure swarms: Theistareykir, Krafla, Fremri-Namur, Askja, and
285 Kverkfjöll (Figure 8A). Extension in these zones is accommodated by systems of normal faults,
286 sub-parallel eruptive fissures, and extension fractures that radiate outward from axial volcanoes in
287 a direction orthogonal to the regional minimum horizontal stress (e.g. Sæmundsson, 1974;
288 Brandsdóttir and Einarsson, 1979). The Krafla central volcano and associated fault and fracture
289 networks have dominated volcanic activity in the axial rift zone, with approximately 35 Holocene
290 basaltic eruptions identified (Brandsdóttir and Einarsson, 1979; Opheim and Gudmundsson,
291 1989). The rift zone extends 80-100 km along strike (Figure 8A), with a width of 4-10 km
292 (Bjornsson et al., 2007).

293

294 *FIGURE 8 HERE*

295

296 Magma is stored beneath the central volcano, in a reservoir at approximately 2.5-3.0 km depth and
297 supplied at a rate of ~1.6 km³ per year (Tryggvason, 1986; Dauteuil et al., 2001). Records of ground
298 deformation, dating back to 1976, highlight pronounced and repeated episodes of steady inflation

309 followed by rapid deflation (and subsidence), associated with rift zone extension (Bjornsson et al.,
300 1978; Tryggvason, 1984; Rubin, 1992). The scale and duration of these episodes is highly variable.
301 For instance, 30-40 x 10⁶ m³ was erupted from Krafla in 1980 over a period of 12 hours. In another
302 episode deflation of the summit reservoir released 198 x 10⁶ m³ over 39 days. During those events,
303 large portions of the rift zone are known to have extended: between 1974-78, up to eight separate
304 inflation-deflation events were recorded and 80-90 km of the ~100 km long rift zone
305 accommodated extension (Tryggvason, 1984). Lateral dyke propagation has been recorded for
306 large distances (~50 km) along the rift zone (Bjornsson et al., 1978; Buck et al., 2006; Hjartardóttir
307 et al., 2012). Based on the ages for lava flows and erosional surfaces, deformation rates are
308 estimated to be between 1.5-15 cm/y⁻¹ (Dauteuil et al., 2001).

309

310 **3.2.1. Surface structures in the Krafla fissure swarm**

311 Here we focus on an area of the Krafla rift system ~10 km north of Krafla Volcano (Figure 8B,
312 C). Mapping reveals the following structures (Figure 8C): (1) first-order rift zone-parallel (NNE-
313 SSW strike) faults, with sub-vertical scarps that dip to the WNW and ESE, and accommodate
314 displacements >15 m; (2) second-order fractures that form linear zones, dominantly within the
315 footwall (and less commonly in the hanging wall); and (3) rare monoclinial folds and hanging wall
316 buckles. Second-order fractures can be grouped into three dominant strike orientations: NNE-SSW
317 (rift-parallel), NW-SE (rift-oblique), and WNW-ESE (rift-normal). Importantly, fractures with
318 orientations outside of the principal rift trend (NNE-SSW) are not randomly distributed but show
319 a close spatial association with the tips of en echelon rift faults (Bubeck et al. in review).

320 Second-order extension fractures in the Krafla fissure swarm form linear zones that are up
321 to 5 km long and 5-15 m wide, dominantly in the footwalls of rift-parallel normal fault segments.

322 Rift-parallel striking fractures of this order are most common in the study area (~60% of mapped
323 fracture traces) and show lengths of up to ~800 m, with apertures of up to 4 m, but commonly in
324 the range 1.0-1.5 m. Rift-oblique (NW-SE) striking fractures are less frequent (~30% of mapped
325 fracture traces), but accommodate similar scales of opening (up to 4 m; modal opening is 2.0-2.5
326 m) across open fault scarps, with lengths up to ~50 m. The walls of fractures in this trend show
327 either left- or right-lateral strike-slip components of displacement in addition to horizontal
328 opening; hence they represent extensional shear fractures. Rift-normal (WNW-ESE) striking
329 fractures are least common (~10% of mapped fracture traces) and show the smallest lengths (less
330 than ~40 m) and apertures (up to ~1 m). None of the fracture sets identified show a preferred
331 stepping direction, and individual fractures show prominent obliquely-oriented steps in their
332 traces, which commonly coincide with points of aperture minima. Such patterns have been
333 interpreted previously elsewhere to represent sites of segment linkage between originally
334 segmented structures (e.g. Peacock and Sanderson, 1991). At the scale of whole fractures (tens to
335 hundreds of metre scale), traces are linear and considered composite structures: i.e. they represent
336 coalesced fractures that were originally segmented.

337

338 *FIGURE 9 HERE*

339

340 Extension in the Krafla fissure swarm is accommodated dominantly by large (>15 m
341 displacement), sub-vertical surface-breaking faults that offset planar footwall-hanging wall surfaces
342 (Figure 9). Faults are continuous in length for 0.5-1.5 km and parallel to the NNE-SSW trend of the
343 rift zone, accommodating WNW-ESE extension (Figure 8B, C). As observed in the Koa'e fault
344 system, faults show significant horizontal openings of up to 4 m, in addition to a vertical component

345 of displacement (Figure 9). A sub-set of shorter normal faults (<0.5 km length) and fractures, which
346 strike at a low angle to the main rift trend (i.e. NW-SE), occurs at the terminations of first-order rift-
347 parallel faults (e.g. Figure 9B). Fractures in this trend show prominent strike-slip displacements.
348 Lateral slip has not been observed across NW-SE striking fault segments, however it should be
349 noted that the lack of preserved piercing points precludes documentation of any lateral component
350 of motion in this case.

351 Crests of monoclines are parallel to the NNE-SSW trend of the rift zone and strike of the
352 first-order normal faults (Figure 10). Based on their spatial extent, only laterally discontinuous
353 (<50 in length) monoclines are identified. Monoclines in the Krafla fissure swarm typically have
354 low amplitudes (<10 m) and rounded morphologies, with open fractures along the upper limb,
355 which are collinear with adjacent open normal fault scarps on either side of the monocline (Figure
356 10A). Breached monoclines are more common in the Krafla study area.

357

358 *FIGURE 10 HERE*

359

360 Where monoclines are breached, amplitudes are generally low (<2 m) and extensional strains have
361 localised on the breaching fault segment, which in some instances, have accrued throws of 0.5-1.0
362 m (e.g. Figure 10B). Along one fault segment there is also evidence for multiple monocline
363 geometries with the development of an additional fold further into the hanging wall, ahead of a
364 breached monocline (Figure 10B). Instances of heavily fractured or disintegrated morphologies,
365 though less common in the Krafla study area, show steep rotations of up to 90° (Figure 10C).
366 Importantly, monoclines in the Krafla fissure swarm are comparatively rare and are associated

367 with smaller rift-parallel striking faults (throw <15 m), rather than representing characteristic
368 features of all faults.

369

370 **4. Discussion**

371 **4.1. Comparison of surface structures in the Koa'e and Krafla fault systems**

372 Field observations of the distribution and geometry of normal faults in the Koa'e fault system and
373 the Krafla fissure swarm show some similar structural features to one another, and to existing
374 predicted geometries (e.g. Grant and Kattenhorn, 2004; Holland et al., 2006; Martel and Langley,
375 2006; Kaven and Martel, 2007), including: (1) sub-vertical fault scarps with prominent openings
376 (2-4 m); (2) monoclines that strike parallel to first-order faults and decrease in width as they
377 increase in height prior to breaching; and (3) zones of sub-vertical fractures that appear to activate
378 pre-existing cooling joints, dominantly in the footwalls of faults, or along the upper limb of
379 monoclines. These shared structural features are predicted to follow a stepwise and systematic
380 evolution with earlier features evident in advanced stages (e.g. Martel and Langley, 2006; Kaven
381 and Martel, 2007).

382 In general, surface-breaking faults in the Krafla fissure swarm are larger (>15 m throw),
383 longer (>500 m) and more prevalent than surface-breaking faults in the Koa'e. Extension fracture
384 networks in the Koa'e are more distributed and comprise a greater number of shorter (between 10-
385 20 m) and smaller (typically 0.3-0.6 m aperture) fractures. These characteristics lead us to consider
386 that faults in the Krafla fissure swarm represent more evolved equivalents of faults in the Koa'e
387 fault system. We might therefore expect faults in both settings to follow the same evolutionary
388 path, as has been suggested previously (e.g., Martel and Langley, 2006), with faults in Krafla to
389 be in a more advanced stage of the same development process.

390 Our field observations, however, highlight prominent departures from both the predicted
391 geometries in the models, and between the two locations; specifically, precursory monoclines are
392 not present along all fault traces, where they ought to be systematically breached. In the Koa‘e
393 fault system, monoclines are not uniformly distributed, but rather they are restricted to central-
394 western and western regions of the fault system (Figure 2B), where they form continuous structural
395 features for up to ~3 km; amplitudes are similar to the surface-breaking fault segments in the
396 eastern portions of the fault system. In the east of the fault system, within ~5 km of the upper ERZ,
397 large (5-15 m throw) surface-breaking faults dominate and outcrop as subvertical, open scarps with
398 few instances of flexure of the ground surface prior to breaching. The result of this distribution of
399 deformation in the Koa‘e is a pronounced east-west structure gradient. In the Krafla fissure swarm,
400 monoclines are comparatively rare and associated with smaller displacement faults. They do not
401 demonstrate a preferred spatial distribution. Surface-breaking normal faults on the other hand, are
402 found up to 20 km away from the central volcano.

403

404 **4.2. Controls on the surface expression of extensional structures**

405 **4.2.1. Syntectonic volcanism**

406 Most numerical and scaled-analogue models of fault growth in cohesive sequences involve
407 uniform, constant-rate displacement boundary conditions (e.g. Grant and Kattenhorn, 2004;
408 Holland et al., 2006, 2011; Martel and Langley, 2006). Driving stresses, and hence, strain rates in
409 both the Koa‘e and Krafla rift settings, however, are neither uniformly distributed, nor constant
410 through time. Extension in both areas is associated with repeated dyke injection events, the scale
411 and timing of which are variable in time, space, and magnitude (e.g. Tryggvason, 1984; Dvorak
412 and Dzurisin, 1993; Bjornsson et al., 2007; Delaney et al., 1998; Buck et al., 2006). Variable rates

413 and duration of magma emplacement within the rift zones has the effect of altering local stress
414 distributions, which in turn drives variations in strain rate and results in local strain rate gradients.
415 This should be expected to influence segmentation patterns and fault architecture. The distribution
416 of surface deformation styles in the Koa‘e fault system may be a record of this.

417

418 *FIGURE 11 HERE*

419

420 Periods of inflation and deflation within Kīlauea ’s south flank have been linked with
421 regions of elevated concomitant seismicity below the summit and upper ERZ (Figure 11) at ~2-
422 3.5 km depth (e.g. Delaney et al., 1998; Hansen et al., 2004; Baker and Amelung, 2012, Lin and
423 Okubo, 2016). Earthquake swarms originating in the upper ERZ have been recorded to migrate
424 into the Koa‘e fault system during intrusion events (Delaney et al., 1998), and in some instances
425 linked to episodes of slip on major faults in the areas. The proximal distribution of surface-breaking
426 faults in the eastern Koa‘e fault system are therefore likely to be linked to these areas of elevated
427 seismicity and magma emplacement. For instance, records of GPS data, InSAR, and field
428 observations, have revealed evidence for minor slip on the Kulanaokuaiki Fault during the
429 September 1999 dyke intrusion event (Cervelli et al., 2002) (Figure 11). This is consistent with
430 elastic dislocation models of the south flank that predict regions of high tensile stress
431 concentrations that centre on the intruded region and extend into the eastern Koa‘e (Owen et al
432 2000; Cervelli et al., 2002). The scale and distribution of such stress concentrations become a
433 function of the magnitude and location of the emplacement event, and hence, the resulting strain
434 rate along the rift zone will vary accordingly. Magmatic and seismic activity in Kīlauea ’s SWRZ,
435 by comparison, is significantly less active (e.g. Dvorak and Dzurisin, 1993; Wauthier et al., 2016).

436 During the period 2005-2007 inflation episode, for example, seismicity records indicate up to ~10
437 events per day in the SWRZ, compared to ~30 per day in the ERZ (Wauthier et al., 2016). Models
438 of magma partitioning suggest that during the period 1840-1989, ~57% of magma supplied to the
439 volcano was emplaced and erupted within the ERZ ($1575 \times 10^6 \text{ m}^3$) with only ~2% ($45 \times 10^6 \text{ m}^3$)
440 being erupted in the SWRZ (Dzurisin et al., 1984; Dvorak and Dzurisin, 1993). The result of this
441 partitioning has led to more than 20 eruptions in the ERZ since 1950, associated with deflation of
442 Kīlauea 's summit reservoir, and only two events taking place in the SWRZ. Partitioning of
443 extensional strain across the Koa'e fault system implies that total strains are comparable across the
444 system, but spatially variable strain rates control whether faults are able to propagate straight to
445 the surface (eastern Koa'e), or remain segmented at depth for protracted periods with slip
446 accommodated aseismically, generating surface monoclines (western Koa'e). This is consistent
447 with volcano-tectonic seismicity modelling from Kīlauea (Wauthier et al., 2016), and other
448 volcanic faults (Toda et al., 2002; Roman and Gardine, 2013), which suggest that low rates of
449 magma emplacement produce correspondingly low strain rates that are unable to drive significant
450 seismicity. With renewed magmatic partitioning into the SWRZ during future episodes, faults in
451 western portions of the Koa'e may therefore breach the surface and monoclines will be preserved
452 in their hanging walls.

453 In contrast, the relatively minor abundance of monoclines and dominance of larger (>10 m
454 throw) surface-breaking faults in the Krafla fissure swarm, up to 20 km away from the summit
455 does not imply the presence of a *spatial* strain rate gradient, indicating magma supply here and
456 related stresses are relatively uniform. Following re-surfacing, therefore, stresses and strain rates
457 are high enough for fault segments to link and propagate straight to the surface without flexing it
458 first. The occurrence, however, of breached monoclines, though uncommon, suggests a temporal

459 strain rate gradient can also exist. In evolving volcanic rift systems, therefore, the final geometry
460 of first-order faults becomes a strain rate-dependent function of the magmatic processes taking
461 place. This dependence becomes both a spatial problem as well as a temporal one.

462

463 **4.2.2. Mechanical stratigraphy**

464 In addition to magmatically induced segmentation patterns, host rock mechanical properties are
465 also likely to play a role in the distribution and geometry of faults in the study areas. A prominent
466 cooling joint fabric and mechanical layers, in the form of bedding and physical property variations
467 (e.g. Planke, 1994; Bubeck et al., 2017), mean that basaltic sequences are highly anisotropic and
468 host a similarly pronounced mechanical stratigraphy as have been reported for layered clastic (e.g.
469 Ferrill et al., 2017) and crystalline-clastic sequences (Walker et al., 2013). Existing studies of
470 extensional fault geometry in mechanically layered sequences have shown that the mechanical
471 properties of a deforming volume will govern segmentation patterns, and hence, the final
472 architecture of fault zones (e.g. Peacock and Sanderson, 1991; Ferrill and Morris, 2003; Schöpfer
473 et al., 2006; Walker et al., 2013). At the metre-scale, anisotropy within basaltic sequences pertains
474 to varying physical and mechanical properties within individual lava units or volcanoclastic
475 horizons, as well as networks of pre-existing cooling joints. At the tens to hundreds of metre-scale,
476 changes in compositional layering and fluid content within the sequence should also be expected
477 to influence the distribution and geometry of surface structures in developing volcanic rift systems.

478

479 **4.3.A modified conceptual model for near-surface fault growth in basaltic sequences**

480 Here we present conceptual models for near-surface fault growth, based on the natural distribution
481 and geometry of extensional structures in the Koa'e and Krafla fault systems, as an expansion of

482 the numerical models presented by Martel and Langley (2006) and Kaven and Martel (2007). As
483 this model is based on surface observations only, stage I is based on theoretical models of dyke-
484 fault relationships from volcanic settings. Depending on the distribution, magnitude, and duration
485 of individual rifting episodes, fault style may show distinct variation as a function of spatial and
486 temporal strain rate evolution. For this reason, stage III of this model is divided into two paths that
487 are referred to here as: a high strain rate path and a low strain rate path.

488

489 *FIGURE 12 HERE*

490

491 **Stage I:** Initial extension may result from magma release during deflation of the central reservoir
492 where high magma pressure will drive dykes into existing adjacent joints or discontinuities. At
493 intermediate depths, upward (or lateral) propagation, governed by the hydrofracture criterion (e.g.
494 Gudmundsson, 2011), is impeded by the presence of mechanical barriers (e.g. Bell and Kilburn,
495 2012) or when driving pressures drop (e.g. Buck et al., 2006; Rowland et al., 2007). Dyke tip
496 stresses are relieved by the growth of normal faults, which propagate along maximum tensile strain
497 trajectories within the overlying basalt cover (e.g. Hollingsworth et al., 2013).

498

499 **Stage II:** In the region ahead of upward-propagating normal faults, at a critical distance from the
500 free surface (controlled by the magnitude of the stress intensity at the fault tip), extension fractures
501 begin to localise in linear zones along pre-existing cooling joints that are optimally oriented. These
502 zones are parallel to the structures at depth and progressively lengthen vertically and laterally
503 (Figure 12A).

504

505 **Stage III (high strain rate):** With continued upward propagation of faults, and downward growth
506 of extension fractures, coalescence and linkage produce through-going faults (Figure 12B). At this
507 stage, extension is localised on a smaller number of larger structures, which dominate over new
508 fracture growth: An exponential scaling is predicted (e.g. Ackerman et al., 2001). During periods
509 of elevated magmatic activity within the rift zone, or in the absence of resistant layers, this process
510 could take place relatively quickly and result in through-going faults without folding of the surface
511 (Figure 12B).

512

513 **Stage III (low strain rate):** During periods, or in regions of subdued magmatism local driving
514 stresses are too low to drive significant fault slip. Under these conditions, through-going linkage
515 is prevented and faults will remain segmented at depth where they will creep aseismically,
516 producing monoclinial folding of the layers ahead of the tip (Figure 12C). With renewed magmatic
517 activity, strain rates will increase once more and through-going segment linkage will be possible.
518 During slip accumulation, and upward propagation, surface monoclines will steepen and become
519 narrower until they are breached along newly linked fault-fracture networks (Figure 12D).

520 In this model, monoclines are not necessarily precursory features of normal fault growth
521 but rather a record of segmented growth, which may develop at any time within the series,
522 depending largely on local strain rates. Breached monoclines, on the other hand, may imply a
523 period, or region, of lower strain rate and segmentation followed by a sudden rate increase once
524 more and through-going fault development. The growth of fault populations through time in
525 developing volcanic rift systems do not follow a uniform, systematic evolution; the distribution
526 and geometry of normal faults in the Krafla fissure swarm are not directly evolved equivalents of
527 faults in the Koa'e fault system. This model may account for the apparent lack of preserved

528 monoclines in exhumed basalt-hosted fault systems (e.g. Walker et al., 2012, 2013). Although
529 factors including pre-existing structures and mechanical stratigraphy will influence the nucleation
530 and initial geometry of fault structures, changes in strain rate at any stage will alter the geometry
531 and distribution of preserved faults. This has important implications for interpretations of faulting
532 at depth and for models of fault development on other planets.

533

534 **5. Conclusions**

535 Current models for surface-breaking in faults in volcanic sequences dominantly invoke geometric
536 or kinematic linkage as a progressive fault zone evolution. We suggest that deviations from model-
537 predicted structural style and distribution can be explained by local variations in strain rate through
538 time, and spatially within the actively deforming region. Surface-breaking faults within individual,
539 or separate rift systems, may not experience a consistent evolution due changes within the
540 magmatic system, and therefore small displacement faults are not necessarily representative of the
541 early stages of more evolved systems.

542

543 **ACKNOWLEDGMENTS**

544 The authors wish to extend enormous gratitude to Don Swanson at the Hawaiian Volcano
545 Observatory, Hawai'i, and Mike Poland (now at Cascades Volcano Observatory, Vancouver) for
546 help and advice during field seasons to the Koa`e fault system. We further thank Don for taking
547 the time to provide feedback on this manuscript and for generously sharing data with us. Authors
548 Bubeck and Walker especially wish to thank Don for an unforgettable first tour of the Koa`e fault
549 system. We also thank the National Park Service for granting a permit to conduct fieldwork in the
550 Koa`e fault system. Aerial LiDAR datasets were provided by the OpenTopography Facility with

551 support from the National Science Foundation under NSF Award Numbers 1226353 & 1225810
552 (not related to this study). This research did not receive any specific grant from funding agencies
553 in the public, commercial, or not-for-profit sectors.

554

555

556 **FIGURES**

557 **Figure 1.** Measurement of fracture geometry and kinematics: extension-mode opening across pre-
558 existing cooling joint surfaces allows the traditional measurement of opening direction, aperture,
559 azimuth and vertical offset (where present).

560

561 **Figure 2.** A) Simplified structural elements map of Kīlauea Volcano: Koa`e fault system (KFS);
562 ERZ: East Rift Zone; SWRZ: Southwest Rift Zone; HFS: Hilina Fault System. Inset shows relative
563 position of A, on the south coast of Hawai‘i. B) Map of extensional structures in the Koa`e fault
564 system: (1) surface-breaking normal faults (yellow lines); (2) extension fracture networks (orange
565 lines); and (3) monoclinial folds with lengths >150 m (green lines). For a colour version of this
566 figure, please refer to the online version.

567

568 **Figure 3.** Scaling and location of extension fracture networks. (A) At the 100’s of metre-scale,
569 fracture zones are predominantly located in the footwall of faults and along the upper limb of
570 monoclines. Zones range from 30-50 in width and extend for >1 km. Base image: aerial World-
571 View 2 satellite image (0.5 m resolution). (B) At the 10’s of metre-scale fractures show stepped
572 geometries and apertures of up to ~4 m. (C) At the cm-scale, fractures also demonstrate stepping
573 trace geometries and “hook-shaped” tip geometries in the vicinity of neighbouring fracture tips.

574 At these scales, fractures are also observed in seemingly undeformed (un-flexed, non-faulted)
575 regions of the fault system.

576

577 **Figure 4.** Examples of monocline type in the Koa'e fault system. (A) Laterally continuous
578 monoclines with fold limbs that dip gently and vary from 2 m to ~ 10 m in amplitude. Zones of
579 fractures are found along the upper limbs and steep, rubbly toes at the base. Crests can be traced
580 for over 1 km. In a small number of cases, minor (<2 m) amounts of throw have been observed
581 across open fractures along the crest. (B) Laterally discontinuous monoclines form densely
582 fractured, often disintegrated blocks in the hanging wall of faults. Lengths vary from 10 m to 150
583 m and amplitudes from 2 m to 15 m. Dashed yellow lines: extent of monocline; dashed red lines:
584 continuous open fracture; dashed blue lines: extent of hanging wall buckles.

585

586 **Figure 5.** Map view of monocline types. (A) a continuous monocline with a network of extension
587 fractures along the upper limb. Limbs dip towards the north at ~10°. Breached continuous
588 monoclines are observed, but less commonly than unbreached. (B) Discontinuous monocline
589 blocks (dotted, yellow lines), isolated between normal fault segments (heavy red line), connected
590 by collinear extension fractures (dotted red line) along the upper limb to form continuous open
591 fractures that decouple the monocline from the footwall. These monoclines dip more steeply (~30°)
592 from a central amplitude maxima, to zero at the lateral edges. Breached discontinuous monoclines
593 have not been observed. (C) Fault tip monoclines between en echelon segments along the Ohale
594 Pali. Tip monoclines dip parallel to the bounding segments by ~10°. Base images: aerial World-
595 View 2 satellite image (0.5 m resolution).

596

597 **Figure 6.** Map view of monocline types moving east along the Ohale Pali (A-D). Solid yellow
598 lines indicate cross-section transects for measurement of transverse width (i-iv). Base images:
599 aerial World-View 2 satellite image (0.5 m resolution). Cross-sections derived from an aerial
600 LiDAR dataset (0.5 m resolution) provided by OpenTopography. A. Zone of distributed footwall
601 extension fracturing (max. aperture 4.5 m; most <1.5 m in aperture) towards the western end of
602 the Ohale Pali. Cross-section (i) indicates an approximate monocline width of 45 m. B. Zone of
603 increasingly localised footwall fracturing along upper limb of monocline (A). Cross-section (ii)
604 indicates an approximate monocline width of 30 m. C. Zone of further localized footwall fractures,
605 with greater apertures (up to 4 m). Cross-section (iii) indicates an approximate width of 20 m. D.
606 Normal fault segment breaching monocline. Cross-section (i) indicates an approximate width of
607 15 m.

608
609 **Figure 7.** Examples of surface-breaking normal fault segments in the Koa‘e fault system. (A) The
610 largest vertical offsets (up to ~15 m) and greatest proportion of fault scarps are found on the
611 Kulanaokuaiki (“Small Shaking Spine”) fault. (B) Where present, scarps show a significant
612 component of horizontal opening and offset planar footwall and hanging wall ground surfaces.
613 Also present along many (but not all) faults in the Koa‘e fault system are hanging wall buckles
614 that occur ahead of both fault scarps and monoclinical structures.

615
616 **Figure 8.** (A) Map of Iceland highlighting the major tectonic elements: Reykjanes Ridge (RR);
617 the Kolbeinsey Ridge (KR); West Volcanic Zone (WVZ); East Volcanic Zone (EVZ); Neo-
618 Volcanic Zone (NVZ: the axial rift zone); Askja volcanic centre (As); Fremri-Namur volcanic
619 centre (Fr); Krafla volcanic centre (Kr); Theistareykir volcanic centre (Th); the Dalvik lineament

620 (DF), the Husavik-Flatey Fault (HF) and the Grimsey lineament (GF). (B) Location of study area
621 in the Gjastykki Valley within the Krafla fissure swarm. (C) Mapped faults and extension/oblique-
622 extensional fractures in the study area.

623

624 **Figure 9.** Examples of surface-breaking normal fault segments in the Gjastykki area of the Krafla
625 fissure swarm. (A) Subvertical normal faults demonstrate throws of up to 25-30 m and offset planar
626 footwall and hanging wall surfaces. (B) Rift faults show prominent horizontal openings of 2-4 m
627 and overlapping geometries with obliquely-oriented linking segments.

628

629 **Figure 10.** Examples of monoclines in the Krafla fissure swarm. (A) Monoclines show amplitudes
630 of up to ~3 m with open fractures along their upper limbs that are co-linear with fault segments on
631 either side. (B) Breached monocline observed in the hanging wall of a surface-breaking normal
632 fault with vertical offset of up 2-3 m. Along the fault in the image, an additional monocline has
633 developed further into the hanging wall. (C) Monoclines can also be strongly fragmented and show
634 steep rotations. In all examples, their lateral extent is <50 m.

635

636 **Figure 11.** Distribution of surface-breaking normal faults and monoclinical folds across the Koa'e
637 fault system. Blue circles represent earthquake epicenters in the summit, upper ERZ and upper
638 SWRZ regions of Kilauea 's south flank from the period 1986-2009. Contours highlight the density
639 of events based on approx. 3000 studied earthquakes recorded in this region (red: high frequency;
640 blue: low frequency). Earthquake data reproduced from Lin and Okubo, 2016. Dyke intrusion
641 events taken from Baker and Amelung, 2015 and Cervelli et al., 2002. For a colour version of this
642 figure, please refer to the online version.

643

644 **Figure 12.** Conceptual model for growth faults in volcanic rift zones with spatially (and
645 temporally) variable strain rates. A) Precursory extension fractures localize in narrow zones at the
646 free surface ahead of blind normal faults. B) in regions of the rift zone where strain rates are high,
647 normal faults propagate straight through the sequence and link with surface fractures, producing
648 fault scarps. A lack of preserved monocline indicates strain rates have remained high since the last
649 resurfacing event. Antithetic faults may develop from points of stress concentration, causing a
650 rotation of the hanging wall block above them. C) in regions of the rift zone where strain rates are
651 low, faults remain segmented at depth where they accumulate slip asecimically and gradually
652 deform the free surface ahead of the tipline into monoclines. D) in regions of the rift zone that
653 experience episodically high strain rates, faults may spend protracted periods segmented at depth,
654 followed by a rapid propagation phase that results in breaching of earlier formed monoclines at
655 the free surface.

656

657 REFERENCES CITED

- 658 1. Segall, P. & Pollard, D. D. 1980. Mechanics of discontinuous faults. *Journal of*
659 *Geophysical Research*, 85, 4337-4350.
- 660 2. Peacock, D. C. P. 2002. Propagation, interaction and linkage in normal fault systems.
661 *Earth Science Reviews*, 58, 121-142.
- 662 3. Long, J. J. & Imber, J. 2010. Geometrically coherent continuous deformation in the
663 volume surrounding a seismically imaged normal fault-array. *Journal of Structural*
664 *Geology*, 32, 222-234.

- 665 4. Morley, C. K., Nelson, R. A., Patton, T. I. & Munn, S. G. 1990. Transfer zones in the East
666 Africa Rift System and their relevance to hydrocarbon exploration in rifts. *The American*
667 *Association of Petroleum Geologists Bulletin*, 74, 1234-1253.
- 668 5. Faulds, J. E. & Varga, R. J. 1998. The role of accommodation zones and transfer zones in
669 the regional segmentation of extended terranes. In: Faulds, J. E and Stewart, J. H. (eds.)
670 Accommodation Zones and Transfer Zones: the Regional Segmentation of the Basin and
671 Range Province: Boulder, Colorado. *Geological Society of America Special Paper* 323, 1-
672 45.
- 673 6. Lambiase, J. J. & Bosworth, W. 1995. Structural controls on sedimentation in continental
674 rifts. In: LAMBIASE, J. J. (ed.) Hydrocarbon habitat in rift basins. Geological Society
675 Special Publication no. 80. The Geological Society, London.
- 676 7. Sharp, I., Gawthorpe, R. L., Armstrong, B. & Underhill, J. R. 2000. Propagation history
677 and passive rotation of mesoscale normal faults: implications for syn-rift stratigraphic
678 development. *Basin Research*, 12, 285-305.
- 679 8. Hus, R., De Batist, M., Klerkx, J. & Matton, C. 2006. Fault linkage in continental rifts:
680 structure and evolution of a large relay ramp in Zavarotny; Lake Baikal (Russia). *Journal*
681 *of Structural Geology*, 28, 1338-1351.
- 682 9. Manzocchi, T., Childs, C. & Walsh, J. J. 2010. Faults and fault properties in hydrocarbon
683 flow models. *Geofluids*, No. 10, 94-113.
- 684 10. Seebeck, H., Nicol, A., Walsh, J. J., Childs, C., Beetham, R. D. & Pettinga, J. 2014. Fluid
685 flow in fault zones from an active rift. *Journal of Structural Geology*, 62, 52-64.
- 686 11. Ferrill, D. A. & Morris, A. P. 2001. Displacement gradient and deformation in normal
687 fault systems. *Journal of Structural Geology*, 23, 619-638.

- 688 12. Walsh, J. J., Bailey, W. R., Childs, C., Nicol, A. & Bonson, C. G. 2003. Formation of
689 segmented normal faults: a 3D perspective. *Journal of Structural Geology*, 25, 1251-1262.
- 690 13. Nixon, C. W., Sanderson, D. J., Dee, S. J., Bull, J. M., Humphreys, R. J. & Swanson, M.
691 H. 2014. Fault interactions and reactivation within a normal-fault network at Milne Point,
692 Alaska. *The American Association of Petroleum Geologists Bulletin*, 98, 2081-2107.
- 693 14. Holland, M., Urai, J. L. & Martel, S. J. 2006. The internal structure of fault zones in
694 basaltic sequences. *Earth and Planetary Science Letters*, 248, 301-315.
- 695 15. Tentler, T. & Acocella, V. 2010. How does the initial configuration of oceanic ridge
696 segments affect their interaction? Insights from analogue models. *Journal of Geophysical*
697 *Research*, 115, 1-16.
- 698 16. Crider, J. G. & Pollard, D. D. 1998. Fault linkage: Three-dimensional mechanical
699 interaction between echelon normal faults. *Journal of Geophysical Research*, 103, 24,373-
700 24,391.
- 701 17. Maerten, L., Gillespie, P. & Pollard, D. D. 2002. Effects of local stress perturbation on
702 secondary fault development. *Journal of Structural Geology*, 24, 145-153.
- 703 18. Schöpfer, M. P. J., Childs, C. & Walsh, J. J. 2006. Localisation of normal faults in
704 multilayer sequences. *Journal of Structural Geology*, 28, 816-833.
- 705 19. Peacock, D. C. P. & Parfitt, E. A. 2002. Active relay ramps and normal fault propagation
706 on Kilauea Volcano, Hawaii. *Journal of Structural Geology*, 24, 729-742.
- 707 20. Martel, S. J. & Langley, J. S. 2006. Propagation of normal faults to the surface in basalt,
708 Koa'e fault system, Hawaii. *Journal of Structural Geology*, 28, 2123-2143.
- 709 21. Kaven, J. O. & Martel, S. J. 2007. Growth of surface-breaching normal faults as a three-
710 dimensional fracturing process. *Journal of Structural Geology*, 29, 1463-1476.

- 711 22. Walker, R. J., Holdsworth, R. E., Imber, J., Faulkner, D. R. & Armitage, P. J. 2013. Fault
712 zone architecture and fluid flow in interlayered basaltic volcanoclastic-crystalline
713 sequences. *Journal of Structural Geology*, 51, 92-104.
- 714 23. Davison, I., Stasiuk, S., Nuttall, P. & Keane, P. 2004. Sub-basalt hydrocarbon prospectivity
715 in the Rockall, Faroe-Shetland and Møre Basins, NE Atlantic. Geological Society London.
716 In: Vining, B.A. and Pickering, S.C. (eds.) *Petroleum Geology: from mature basins to new*
717 *frontiers. Proceedings of the 7th Petroleum Geology Conference*, 1025-1032. Petroleum
718 Geology Conferences Ltd, published by the Geological Society, London.
- 719 24. Walker, R. J., Holdsworth, R. E., Imber, J. & Ellis, D. 2012. Fault-zone evolution in
720 layered basalt sequences: A case study from the Faroe Islands, NE Atlantic margin.
721 *Geological Society of America Bulletin*, 124, 1382-1393.
- 722 25. Anderson, S. R. & Bowers, B. 1995. Stratigraphy of the unsaturated zone and uppermost
723 part of the Snake River Plain aquifer at Test Area North, Idaho National Engineering
724 Laboratory, Idaho. *Water Resources Investigations Report 95-4130. US Geological Survey*.
- 725 26. Helm-Clark, C. M., Rodgers, D. W. & Smith, R. P. 2004. Borehole geophysical techniques
726 to define stratigraphy, alteration and aquifers in basalt. *Journal of Applied Geophysics*, 55,
727 3-38.
- 728 27. Le Corvec, N. & Walter, T. R. 2009. Volcano spreading and fault interaction influenced by
729 rift zone intrusions: Insights from analogue experiments analyzed with digital image
730 correlation technique. *Journal of Volcanology and Geothermal Research*, 183, 170-182.
- 731 28. Plattner, C., Amelung, F., Baker, S., Govers, R. & Poland, M. 2013. The role of viscous
732 magma mush spreading in volcanic flank motion at Kīlauea Volcano, Hawai‘i. *Journal of*
733 *Geophysical Research: Solid Earth*, 118, 2474-2487.

- 734 29. Forslund, T. & Gudmundsson, A. 1991. Crustal spreading due to dikes and faults in
735 southwest Iceland. *Journal of Structural Geology*, 13, 443-457.
- 736 30. Gudmundsson, A. 2011. *Rock Fractures in Geological Processes*, Cambridge, UK,
737 Cambridge University Press.
- 738 31. Grant, J. V. & Kattenhorn, S. A. 2004. Evolution of vertical faults at an extensional plate
739 boundary, southwest Iceland. *Journal of Structural Geology*, 26, 537-557.
- 740 32. Duffield, W. A. 1975. Structure and Origin of the Koa'e Fault System, Kilauea Volcano,
741 Hawaii. *Geological Survey Professional Paper 856*.
- 742 33. Acocella, V., Gudmundsson, A. & Funicello, R. 2000. Interaction and linkage of extension
743 fractures and normal faults: examples from the rift zone of Iceland. *Journal of Structural*
744 *Geology*, 22, 1233-1246.
- 745 34. Villemin, T. & Bergerat, F. 2013. From surface fault traces to a fault growth model: The
746 Vogar Fissure Swarm of the Reykjanes Peninsula, Southwest Iceland. *Journal of Structural*
747 *Geology*, 51, 38-51.
- 748 35. Opheim, J. A. & Gudmundsson, A. 1989. Formation and geometry of fractures, and related
749 volcanism, of the Krafla fissure swarm, northeast Iceland. *Geological Society of America*
750 *Bulletin*, 101, 1608-1622.
- 751 36. Podolsky, D. M. W. & Roberts, G. P. 2008. Growth of the volcano-flank Koa'e fault system,
752 Hawaii. *Journal of Structural Geology*, 30, 1254-1263.
- 753 37. Casey, M., Ebinger, C., Keir, D., Gloaguen, R. & Mohamed, F. (eds.) 2006. *Strain*
754 *accommodation in transitional rifts: extension by magma intrusion and faulting in*
755 *Ethiopian rift magmatic segments*, The Geological Society of London: Geological
756 Society, London, Special Publications.

- 757 38. Rowland, J. V., Baker, E., Ebinger, C. J., Keir, D., Kidane, T., Biggs, J., Hayward, N. &
758 Wright, T. J. 2007. Fault growth at a nascent slow-spreading ridge: 2005 Dabbahu rifting
759 episode, Afar. *Geophysical Journal International*, 171, 1226-1246.
- 760 39. Soule, S. A., Escartín, J. & Fornari, D. J. 2009. A record of eruption and intrusion at a
761 fast spreading ridge axis: Axial summit trough of the East Pacific Rise at 9-10°N.
762 *Geochemistry, Geophysics, Geosystems*, 10.
- 763 40. Escartín, J., Leclerc, F., Olive, J. A., Mevel, C., Cannat, M., Petersen, S., Augustin, N.,
764 Feuillet, N., Deplus, C., Bezos, A., Bonnemains, D., Chavagnac, V., Choi, Y., Godard,
765 M., Haaga, K. A., Hamelin, C., Ildefonse, B., Jamieson, J. W., John, B. E., Leleu, T.,
766 Macleod, C. J., Massot-Campos, M., Nomikou, P., Paquet, M., Rommevaux-Jestin, C.,
767 Rothenbeck, M., Steinführer, A., Tominaga, M., Triebe, L., Campos, R., Gracias, N.,
768 Garcia, R., Andreani, M. & Vilaseca, G. 2016. First direct observation of coseismic slip
769 and seafloor rupture along a submarine normal fault and implications for fault slip
770 history. *Earth and Planetary Science Letters*, 450, 96-107.
- 771 41. Tanaka, K., Rodriguez, J., Skinnerjr, J., Bourke, M., Fortezzo, C., Herkenhoff, K., Kolb,
772 E. & Okubo, C. 2008. North polar region of Mars: Advances in stratigraphy, structure,
773 and erosional modification. *Icarus*, 196, 318-358.
- 774 42. Nahm, A. L. & Schultz, R. A. 2015. Rupes Recta and the geological history of the Mare
775 Nubium region of the Moon: insights from forward mechanical modelling of the ‘Straight
776 Wall’. *Geological Society, London, Special Publications*, 401, 377-394.
- 777 43. Neal, C. A. & Lockwood, J. P. 2003. Geologic map of the summit region of Kilauea
778 volcano, Hawaii. *USGS Geologic Investigation Series*, I-2759.

- 779 44. Baker, S. & Amelung, F. 2012. Top-down inflation and deflation at the summit of
780 Kīlauea Volcano, Hawai‘i observed with InSAR. *Journal of Geophysical Research: Solid*
781 *Earth*, 117, n/a-n/a.
- 782 45. Lin, G., Amelung, F., Lavallee, Y. & Okubo, P. G. 2014. Seismic evidence for a crustal
783 magma reservoir beneath the upper east rift zone of Kilauea volcano, Hawaii. *Geology*,
784 42, 187-190.
- 785 46. Swanson, D. A., Duffield, W. A. & Fiske, R. S. 1976. Displacement of the south flank of
786 Kilauea Volcano: the result of forceful intrusion of magma into the rift zones. *US Geological*
787 *Survey Professional Paper*, 963.
- 788 47. Dzurisin, D., Koyanagi, R. Y. & English, T. T. 1984. Magma supply and storage at Kilauea
789 Volcano, Hawaii, 1956-1983. *Journal of Volcanology and Geothermal Research*, 21, 177-
790 206.
- 791 48. Poland, M.P., Miklius, A., and Montgomery-Brown, E.K., 2014, Magma supply, storage,
792 and transport at shield-stage Hawai‘ian volcanoes, *in* Poland, M.P., Takahashi, T.J., and
793 Landowski, C.M., eds., *Characteristics of Hawai‘ian volcanoes: U.S. Geological Survey*
794 *Professional Paper 1801*, p. 179–234.
- 795 49. Duffield, W. A., Christiansen, R. L., Koyanagi, R. Y. & Peterson, D. W. 1982a. Storage,
796 migration and eruption of magma at Kilauea Volcano, Hawaii, 1971-1972. *Journal of*
797 *Volcanology and Geothermal Research*, 13, 273-307.
- 798 50. Wright, T. L. & Klein, F. W. 2006. Deep magma transport at Kilauea volcano, Hawaii.
799 *Lithos*, 87, 50-79.
- 800 51. Poland, M. P., Miklius, A., Sutton, A. J. & Thornber, C. R. 2012. A mantle-driven surge in
801 magma supply to Kilauea Volcano during 2003-2007. *Nature Geoscience*, 5, 295-300.

- 802 52. Dvorak, J. J. & Dzurisin, D. 1993. Variations in Magma Supply Rate at Kilauea Volcano,
803 Hawaii. *Journal of Geophysical Research-Solid Earth*, 98, 22255-22268.
- 804 53. Delaney, P. T., Fiske, R. S., Miklius, A., Okamura, A. T. & Sako, M. K. 1990. Deep
805 magma body beneath the summit and rift zones of Kilauea Volcano,
806 Hawaii. *Science* 247.4948 (1990): 1311-1316.
- 807 54. Delaney, P. T., Denlinger, R. P., Lisowski, M., Miklius, A., Okubo, P. G., Okamura, A. T.
808 & Sako, M. K. 1998. Volcanic Spreading at Kilauea, 1976–1996. *Journal of Geophysical*
809 *Research*, 103, 18,003-18,023.
- 810 55. Klein, F. W., Koyanagi, R. Y., Nakata, J. S. & Tanigawa, W. R. 1987. Volcanism in Hawaii.
811 In: Decker, R. W., Wright, T. L. and Stuaffer, P. H. (eds.) US Geological Survey
812 Professional Paper 1350.
- 813 56. Denlinger, R. P. & Okubo, P. G. 1995. Structure of the mobile south flank of Kilauea
814 Volcano, Hawaii. *Journal of Geophysical Research*, 100, 24499.
- 815 57. Bubeck, A., Walker, R. J., Imber, J., Holdsworth, R. E., MacLeod, C. J., and Holwell, D.
816 A.: Rift zone-parallel extension during segmented fault growth: application to the
817 evolution of the NE Atlantic, *Solid Earth Discuss.*, <https://doi.org/10.5194/se-2017-94>, in
818 review, 2017.
- 819 58. Peacock, D. C. P. & Sanderson, D. J. 1991. Displacements, segment linkage and relay ramps
820 in normal fault zones. *Journal of Structural Geology*, 13, 721-733.
- 821 59. Michie, E. a. H., Haines, T. J., Healy, D., Neilson, J. E., Timms, N. E. & Wibberley, C. a.
822 J. 2014. Influence of carbonate facies on fault zone architecture. *Journal of Structural*
823 *Geology*, 65, 82-99.

- 824 60. Lin, G. & Okubo, P. G. 2016. A large refined catalog of earthquake relocations and focal
825 mechanisms for the Island of Hawai‘i and its seismotectonic implications. *Journal of*
826 *Geophysical Research: Solid Earth*.
- 827 61. Sæmundsson, K. 1974. Evolution of the axial rifting zone in northern Iceland and the
828 Tjörnes Fracture Zone. *Geological Society of America Bulletin*, 85, 495-504.
- 829 62. Wright, T. J., Sigmundsson, F., Pagli, C., Belachew, M., Hamling, I. J., Brandsdottir, B.,
830 Keir, A., Pedersen, R., Ayele, A., Ebinger, C., Einarsson, P., Lewi, E. & Calais, E. 2012.
831 Geophysical constraints on the dynamics of spreading centres from rifting episodes on
832 lands. *Nature Geoscience*, 5, 242-250.
- 833 63. Brandsdottir, B. & Einarsson, P. 1979. Seismic activity associated with the September 1977
834 deflation of the Krafla central volcano in north-eastern Iceland. *Journal of Volcanology and*
835 *Geothermal Research*, 6, 197-212.
- 836 64. Bjornsson, A., Saemundsson, K., Sigmundsson, F., Halldorsson, P., Sigbjornsson, R. &
837 Snaebjornsson, J. T. 2007. Geothermal projects in NE Iceland at Krafla, Bjarnarflag,
838 Gjastykki and Theistareykir: assessment of geo-hazards affecting energy production and
839 transmission systems emphasizing structural design criteria and mitigation of risk.
840 Landsvirkjun report LV-2007/075.
- 841 65. Tryggvason, E. 1986. Multiple magma reservoirs in a rift-zone volcano - ground
842 deformation and magma transport during the September 1984 eruption of Krafla, Iceland.
843 *Journal of Volcanology and Geothermal Research*, 28, 1-44.
- 844 66. Dauteuil, O., Angelier, J., Bergerat, F., Verrier, S. & Villemin, T. 2001. Deformation
845 partitioning inside a fissure swarm of the northern icelandic rift. *Journal of Structural*
846 *Geology*, 23, 1359-1372.

- 847 67. Bjornsson, A., Johnsen, G., Sigurdsson, S., Thorbergsson, G. & Tryggvason, E. 1978.
848 Rifting of the plate boundary in North Iceland 1975-1978. National Energy Authority
849 Report OS-JHD-78-21. Nordic Volcanological Institute: University of Iceland.
- 850 68. Tryggvason, E. 1984. Widening of the Krafla fissure swarm during the 1975-1981 volcano-
851 tectonic episode. *Bulletin of Volcanology*, 47-1, 47-69.
- 852 69. Rubin, A. M. 1992. Dike-induced faulting and graben subsidence in volcanic rift zones.
853 *Journal of Geophysical Research: Solid Earth*, 97, 1839-1858.
- 854 70. Buck, W. R., Einarsson, P. & Brandsdóttir, B. 2006. Tectonic stress and magma chamber
855 size as controls on dike propagation: Constraints from the 1975–1984 Krafla rifting episode.
856 *Journal of Geophysical Research*, 111, 1-15.
- 857 71. Hjartardóttir, Á. R., Einarsson, P., Bramham, E. & Wright, T. J. 2012. The Krafla fissure
858 swarm, Iceland, and its formation by rifting events. *Bulletin of Volcanology*, 74, 2139-2153.
- 859 72. Hansen, S., Thurber, M., Mandernach, F., Haslinger, F. & Doran, C. 2004. Seismic
860 velocity and attenuation structure of the East Rift Zone and south flank of Kilauea
861 Volcano, Hawaii. *Bulletin of the seismological society of america*, 94.
- 862 73. Cervelli, P., Segall, P., Amelung, F., Garbeil, H., Meertens, C., Owen, S., Miklius, A. &
863 Lisowski, M. 2002. The 12 September 1999 Upper East Rift Zone dike intrusion at
864 Kilauea Volcano, Hawaii. *Journal of Geophysical Research: Solid Earth*, 107, ECV 3-1-
865 ECV 3-13.
- 866 74. Owen, S., Segall, P., Lisowski, M., Miklius, A., Denlinger, R. P. & Sako, M. 2000. Rapid
867 deformation of Kilauea Volcano: Global Positioning System measurements between
868 1990 and 1996. *Journal of Geophysical Research*, 105, 18983.

- 869 75. Wauthier, C., Roman, D. C. & Poland, M. P. 2016. Joint analysis of geodetic and
870 earthquake fault-plane solution data to constrain magmatic sources: A case study from
871 Kīlauea Volcano. *Earth and Planetary Science Letters*, 455, 38-48.
- 872 76. Toda, S., Stein, R. S. & Sagiya, T. 2002. Evidence from AD 2000 Izu islands earthquake
873 swarm that stressing rate governs seismicity. *Nature*, 419.
- 874 77. Roman, D. C. & Gardine, M. D. 2013. Seismological evidence for long-term and rapidly
875 accelerating magma pressurization preceding the 2009 eruption of Redoubt Volcano,
876 Alaska. *Earth and Planetary Science Letters*, 371-372, 226-234.
- 877 78. Planke, S., Alvestad, E. & Eldhom, O. 1999. Seismic characteristics of basaltic extrusive
878 and intrusive rocks. *The Leading Edge*, 342-348.
- 879 79. Bubeck, A., Walker, R. J., Healy, D., Dobbs, M. & Holwell, D. A. 2017. Pore geometry
880 as a control on rock strength. *Earth and Planetary Science Letters*, 457, 38-48.
- 881 80. Ferrill, D. A., Morris, A. P., McGinnis, R. N., Smart, K. J., Wigginton, S. S. & Hill, N. J.
882 2017. Mechanical stratigraphy and normal faulting. *Journal of Structural Geology*, 94,
883 275-302.
- 884 81. Ferrill, D. A. & Morris, A. P. 2003. Dilational normal faults. *Journal of Structural*
885 *Geology*, 25, 183-196.
- 886 82. Bell, A. F. & Kilburn, C. R. J. 2012. Precursors to dyke-fed eruptions at basaltic
887 volcanoes: insights from patterns of volcano-tectonic seismicity at Kilauea volcano,
888 Hawaii. *Bulletin of Volcanology*, 74, 325-339.
- 889 83. Hollingsworth, J., Leprince, S., Ayoub, F. & Avouac, J. P. 2013. New constraints on dike
890 injection and fault slip during the 1975-1984 Krafla rift crisis, NE Iceland. *Journal of*
891 *Geophysical Research: Solid Earth*, 118, 3707-3727.

892 84. Ackermann, R. V., Schlische, R. W. & Withjack, M. O. 2001. The geometric and
893 statistical evolution of normal fault systems: an experimental study of the effects of
894 mechanical layer thickness on scaling laws. *Journal of Structural Geology*, 23, 1803-
895 1819.
896

Figure 1
W: 84.7 mm
H: 66.7 mm

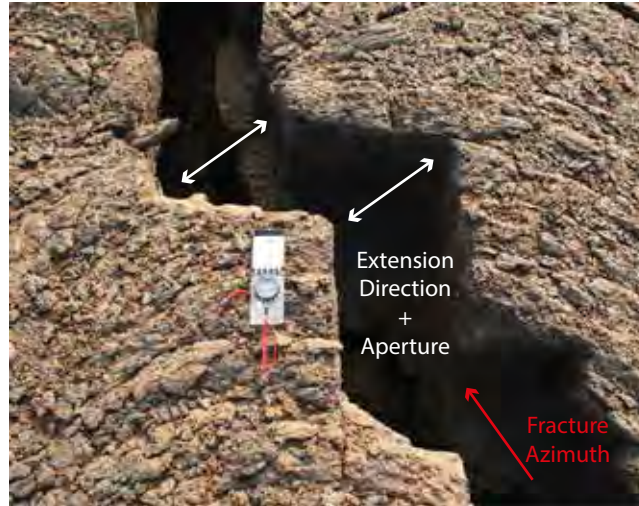


Figure 1. Measurement of fracture geometry and kinematics: extension-mode opening across pre-existing cooling joint surfaces allows the traditional measurement of opening direction, aperture, azimuth and vertical offset (where present).

Figure 2
 W: 120 mm
 H: 95 mm

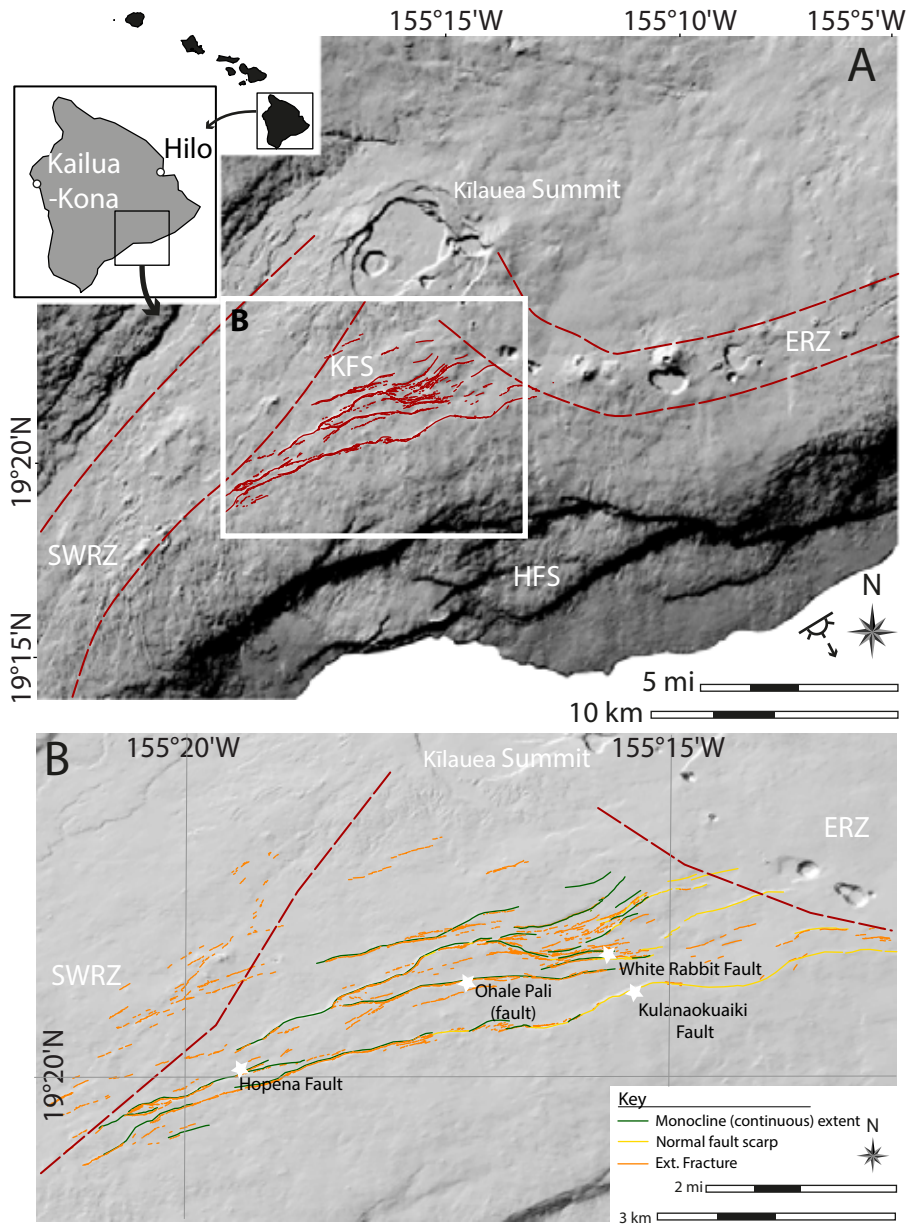


Figure 2. A) Simplified structural elements map of Kilauea Volcano: Koa`e fault system (KFS); ERZ: East Rift Zone; SWRZ: Southwest Rift Zone; HFS: Hilina Fault System. Inset shows relative position of A, on the south coast of Hawai`i. B) Map of extensional structures in the Koa`e fault system: (1) surface-breaking normal faults (yellow lines); (2) extension fracture networks (orange lines); and (3) monoclinical folds with lengths >150 m (green lines).

Figure 3
W: 144.7 mm
H: 177.7 mm

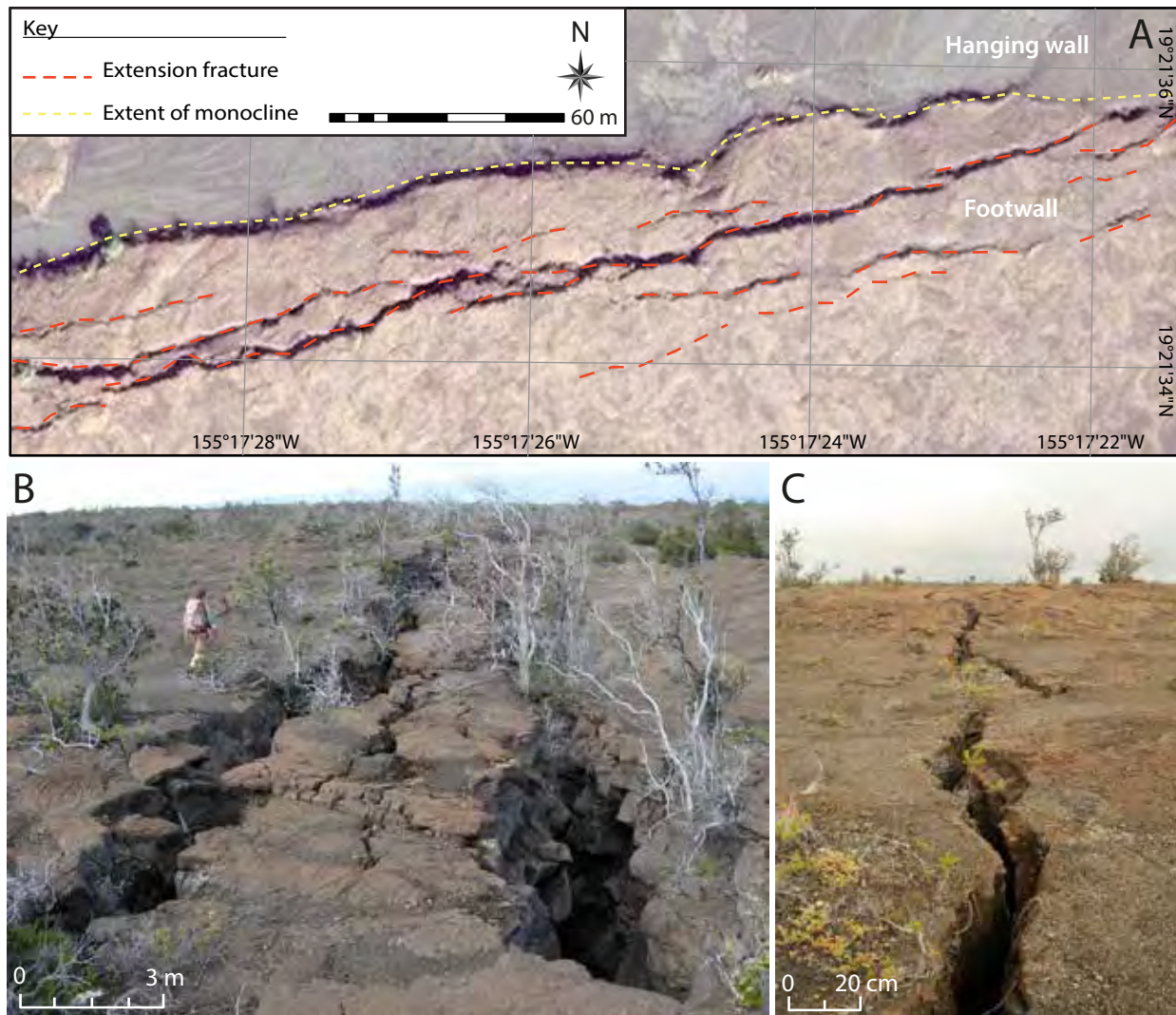


Figure 3. Scaling and location of extension fracture networks. A) At the 100's of metre-scale, fracture zones are predominantly located in the footwall of faults and along the upper limb of monoclines. Zones range from 30-50 m in width and extend for >1 km. Base image: aerial World-View 2 satellite image (0.5 m resolution). B) At the 10's of metre-scale fractures show stepped geometries and apertures of up to ~4 m. C) At the cm-scale, fractures also demonstrate stepping trace geometries and "hook-shaped" tip geometries in the vicinity of neighbouring fracture tips. At these scales, fractures are also observed in otherwise undeformed (i.e. un-flexed, non-faulted) regions of the fault system.

Figure 4
W: 147.7 mm
H: 201 mm

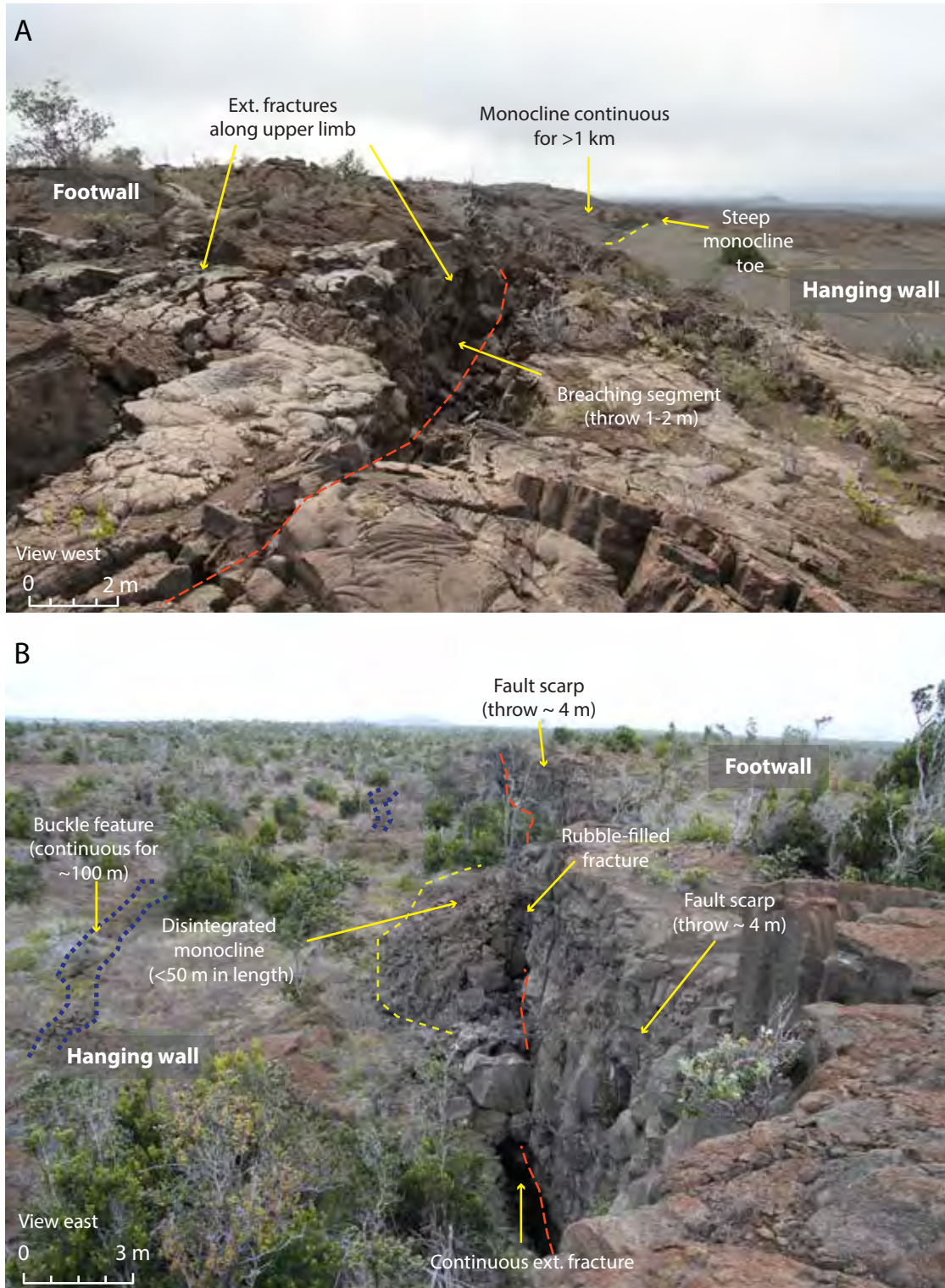


Figure 4. Examples of monocline type in the Koa'e fault system. A) Laterally continuous monoclines with fold limbs that dip gently and vary from a 2 m to ~ 10 m in amplitude. Zones of fractures are found along the upper limbs and steep, rubbly toes at the base. Crests can be traced for over 1 km. In a small number of cases, minor (<2 m) amounts of throw have been observed across open fractures along the crest. B) Laterally discontinuous monoclines form densely fractured, often disintegrated blocks in the hanging wall of faults. Lengths vary from 10 m to 150 m and amplitudes from 2 m to 15 m. Dashed yellow lines: extent of monocline; dashed red lines: continuous open fracture; dashed blue lines: extent of hanging wall buckles.

Figure 5
 W: 157.6 mm
 H: 108.5 mm

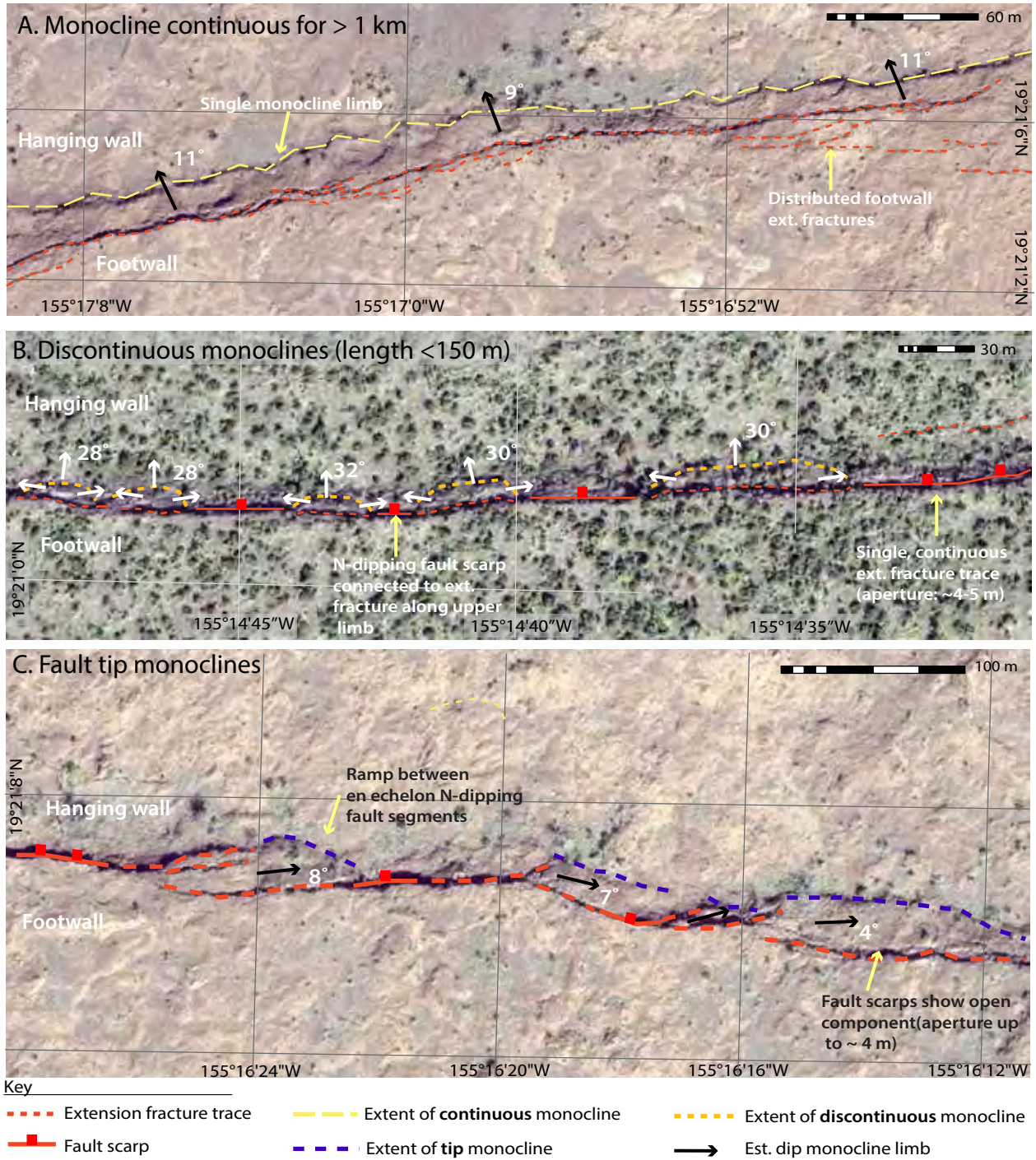


Figure 5. Map view of monocline types. A) a continuous monocline with a network of extension fractures along the upper limb. Limbs dip towards the north at ~10°. Breached continuous monoclines are observed, but less commonly than unbreached. B) Discontinuous monocline blocks (dotted, yellow lines), isolated between normal fault segments (heavy red line), connected by collinear extension fractures (dotted red line) along the upper limb to form continuous open fractures that decouple the monocline from the footwall. These monoclines dip more steeply (~30°) from a central amplitude maxima, to zero at the lateral edges. Breached discontinuous monoclines have not been observed. C) Fault tip monoclines between en echelon segments along the Ohale Fault. Tip monoclines dip parallel to the bounding segments by ~10°. Base images: World-View 2 satellite image (0.5 m resolution).

Figure 6
W: 157.6 mm
H: 108.5 mm

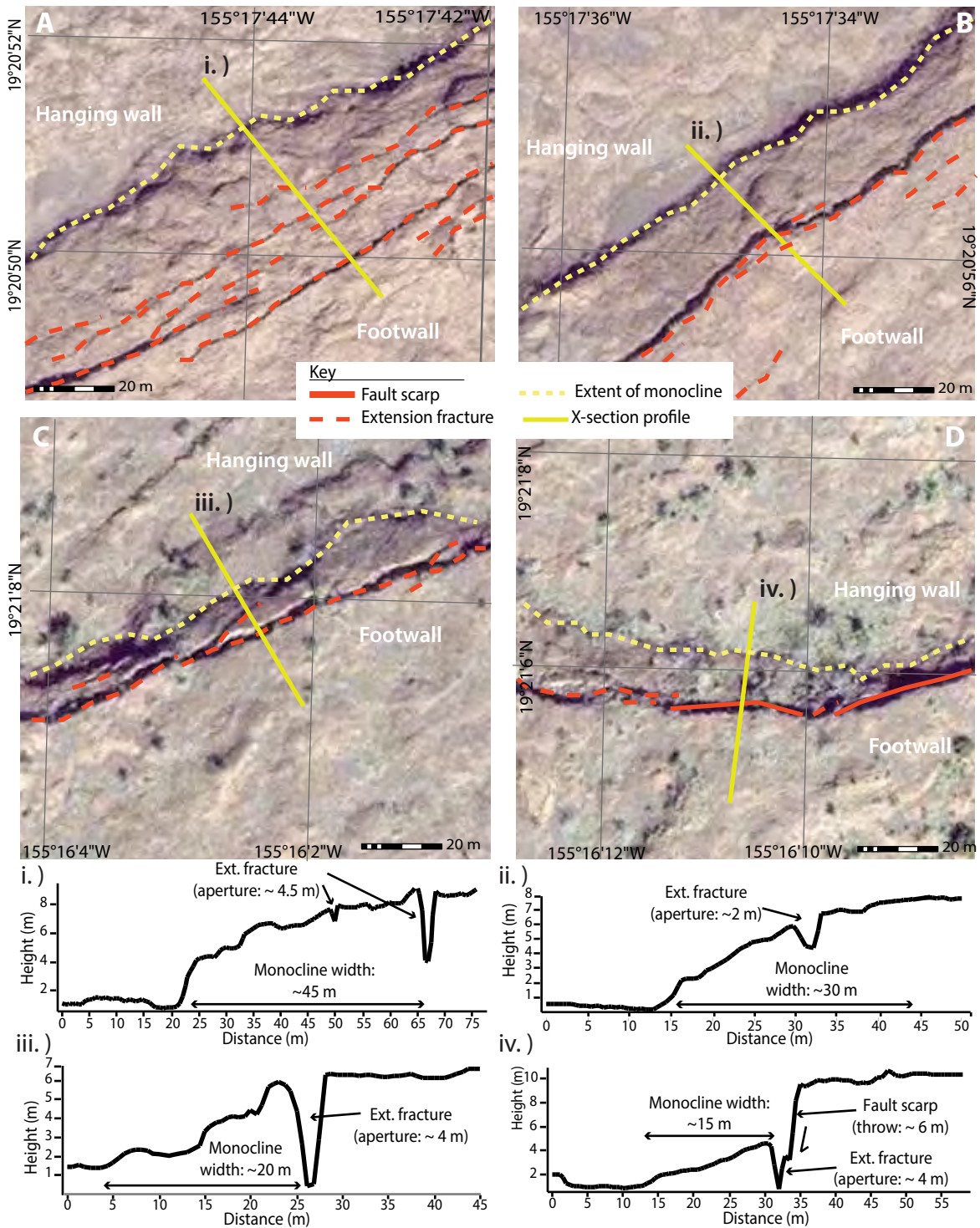


Figure 6. Map view of monocline types moving east along the Ohale Pali (A-D). Solid yellow lines indicate cross-section transects for measurement of transverse width (i-iv). Base images: aerial World-View 2 satellite image (0.5 m resolution). Cross-sections derived from an aerial LiDAR dataset (0.5 m resolution) provided by OpenTopography. A.) Zone of distributed footwall extension fracturing (max. aperture 4.5 m; most <1.5 m in aperture) towards the western end of the Ohale Pali. Cross-section (i) indicates an approximate monocline width of 45 m. B.) Zone of increasingly localised footwall fracturing along upper limb of monocline. Cross-section (ii) indicates an approximate monocline width of 30 m. C.) Zone of further localised footwall fractures, with greater apertures (up to 4 m). Cross-section (iii) indicates an approximate width of 20 m. D.) Normal fault segment breaches monocline. Cross-section (iv) indicates an approximate width of 15 m.

Figure 7
 W: 144.7 mm
 H: 177.7 mm

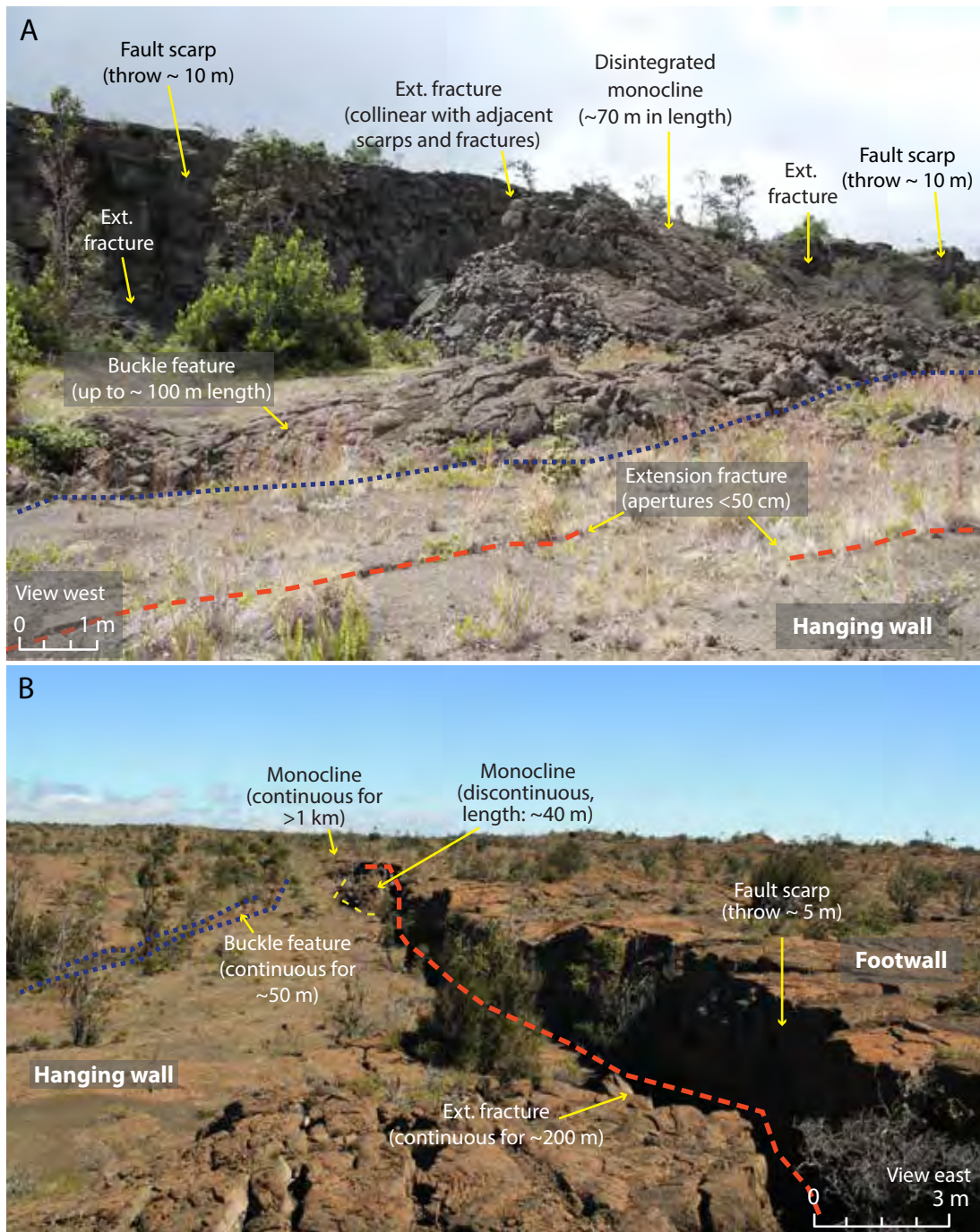


Figure 7. Examples of surface-breaking normal fault segments in the Koa'e fault system. (A) The largest vertical offsets (up to ~15m) and greatest proportion of fault scarps are found on the Kulanaokuaiki ("Small Shaking Spine") fault. (B) Where present, scarps show a significant component of horizontal opening and offset planar footwall and hanging wall ground surfaces. Also present along many (but not all) faults in the Koa'e fault system are hanging wall buckles that occur ahead of both fault scarps and monoclinial structures. Dashed yellow lines: extent of monocline; dashed red lines: continuous open fracture; dashed blue lines: extent of hanging wall buckles.

Figure 8
W: 126.3 mm
H: 115.5 mm

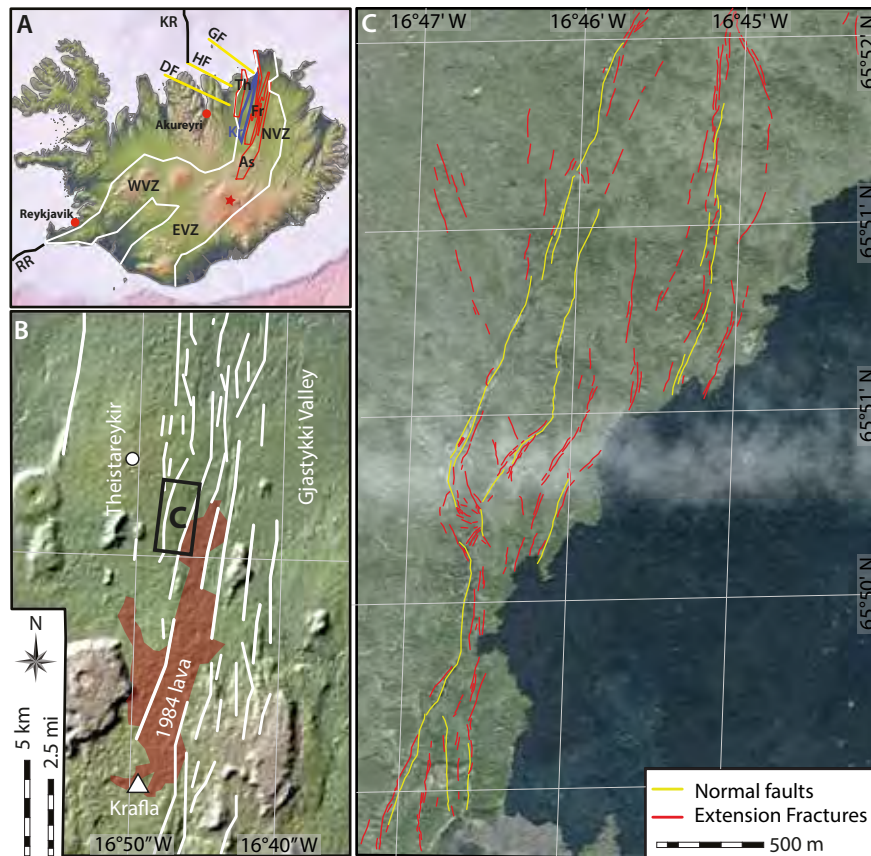


Figure 8. (A) Map of Iceland highlighting the major tectonic elements: Reykjanes Ridge (RR); the Kolbeinsey Ridge (KR); West Volcanic Zone (WVZ); East Volcanic Zone (EVZ); Neo-Volcanic Zone (NVZ: the axial rift zone); Askja volcanic centre (As); Fremri-Namur volcanic centre (Fr); Krafla volcanic centre (Kr); Theistareykir volcanic centre (Th); the Dalvik lineament (DF), the Husavik-Flatey Fault (HF) and the Grimsey lineament (GF). (B) Location of study area in the Gjastykki Valley within the Krafla fissure swarm. (C) Mapped faults and extension/oblique-extensional fractures in the study area.

Figure 9
W: 112mm
H: 159.4 mm



Figure 9. Examples of surface-breaking normal fault segments in the Gjastykki area of the Krafla fissure swarm. (A) Subvertical normal faults demonstrate throws of up to 25-30 m and offset planar footwall and hanging wall surfaces. (B) Rift faults show prominent horizontal openings of 2-4 m and overlapping geometries with obliquely-oriented linking segments.

Figure 10
 W: 99.4 mm
 H: 202.4 mm

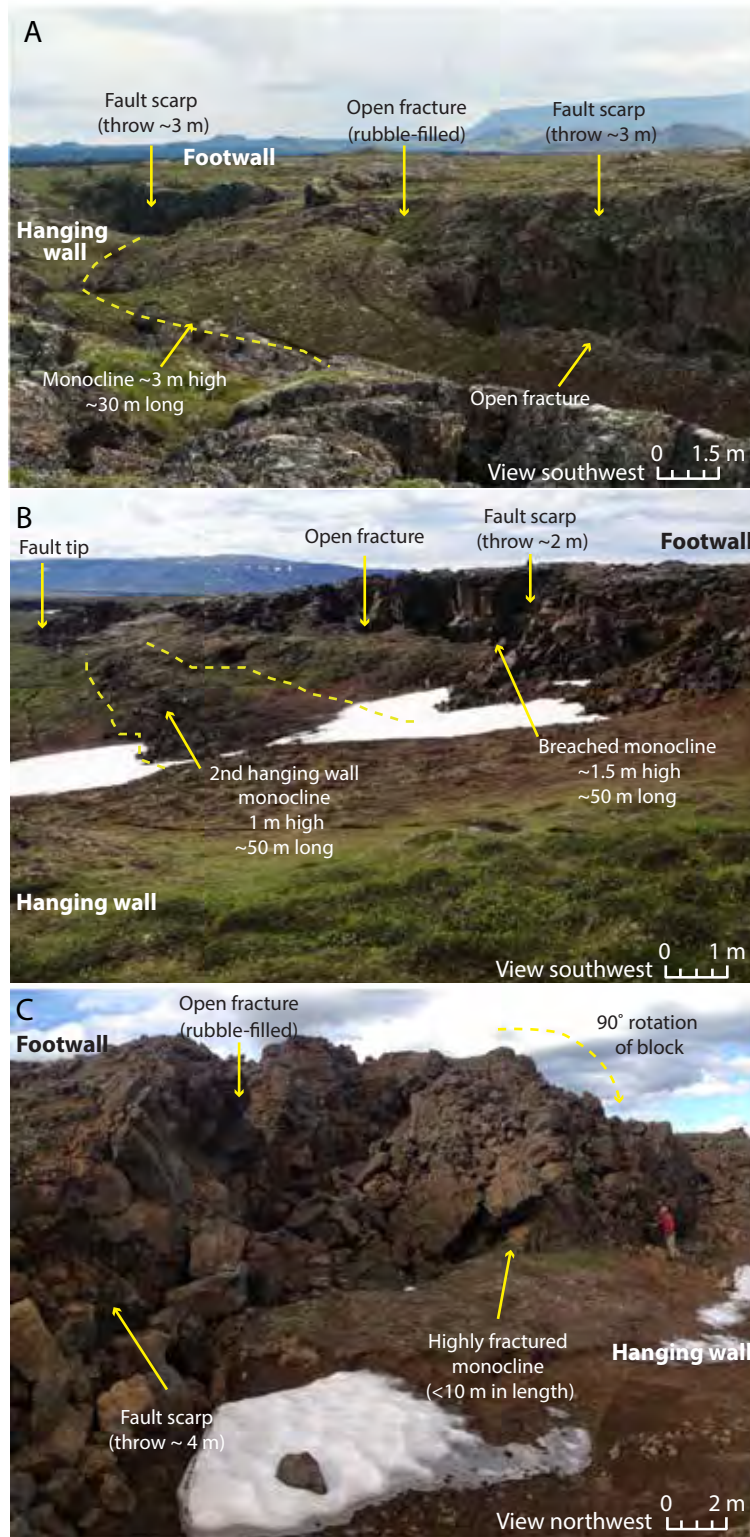


Figure 10. Examples of monoclines in the Krafla fissure swarm. (A) Monoclines show amplitudes of up to ~3 m with open fractures along their upper limbs that are co-linear with fault segments on either side. (B) Breached monocline observed in the hangingwall of a surface-breaking normal fault with vertical offset of up 2-3 m. Along the fault in the image, an additional monocline has developed further into the hangingwall. (C) Monoclines can also be strongly fragmented and show steep rotations. In all examples, their lateral extent is <50 m.

Figure 11
 W: 192 mm
 H: 150 mm

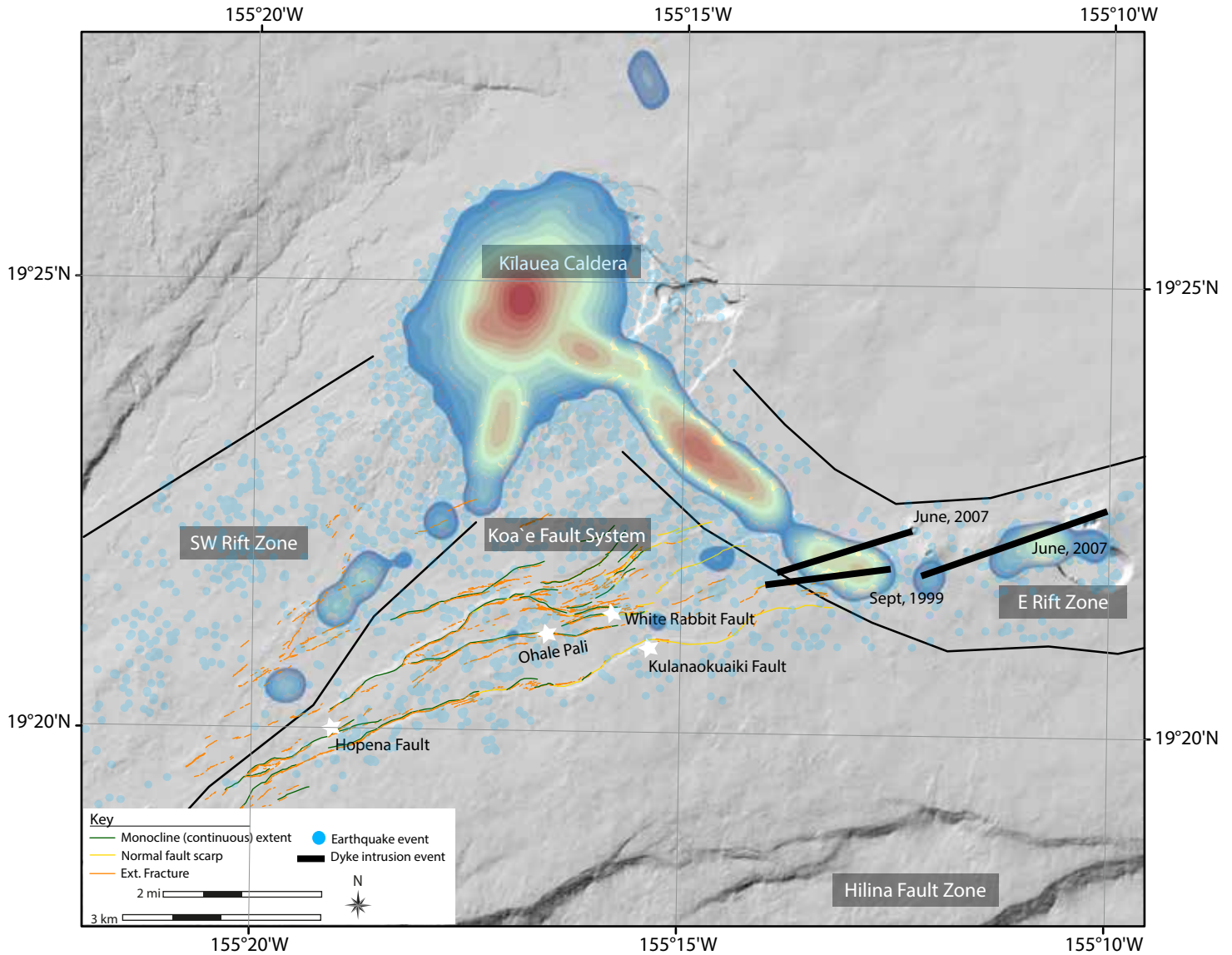


Figure 11. Distribution of surface-breaking normal faults and monoclinical folds across the Koa`e fault system. Blue circles represent focal mechanisms in the summit, upper ERZ and upper SWRZ regions of Kilauea Volcano from the period 1986-2009. Contours highlight the density of events based on approx. 3000 focal mechanisms recorded in this region (red: high frequency; blue: low frequency). Earthquake data reproduced from Lin and Okubo, 2016. Dyke intrusion events taken from Baker and Amelung, 2015 and Cervelli et al., 2002.

Figure 12
W: 154 mm
H: 114 mm

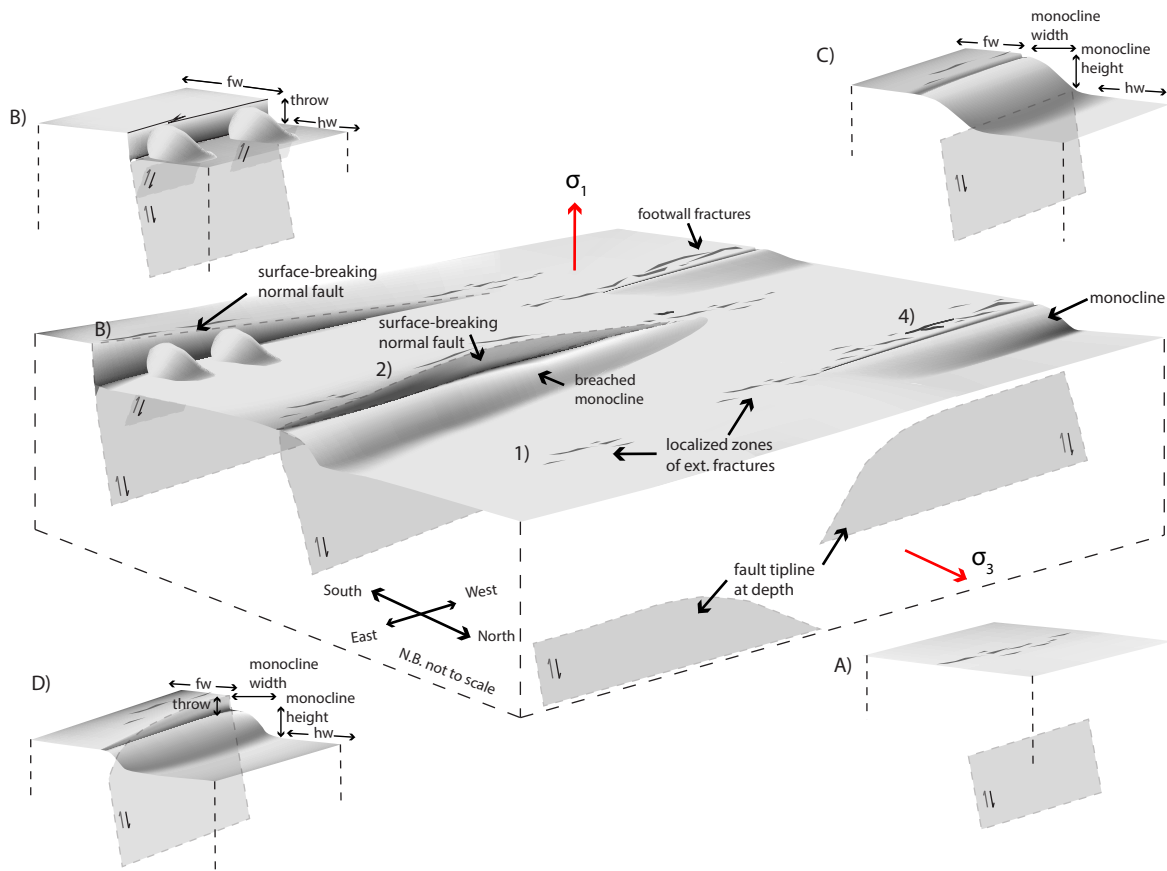


Figure 12. Conceptual model for growth faults in volcanic rift zones with spatially (and temporally) variable strain rates. A) Precursory extension fractures localise in narrow zones at the free surface ahead of blind normal faults. B) in regions of the rift zone where strain rates are high, normal faults propagate straight through the sequence and link with surface fractures, producing fault scarps. A lack of preserved monocline indicates strain rates have remained high since the last resurfacing event. Antithetic faults may develop from points of stress concentration, causing a rotation of the hanging wall block above them. C) in regions of the rift zone where strain rates are low, faults remain segmented at depth where they accumulate slip aperiodically and gradually deform the free surface ahead of the tipline into monoclines. D) in regions of the rift zone that experience episodically high strain rates, faults may spend protracted periods segmented at depth, followed by a rapid propagation phase that results in breaching of earlier formed monoclines at the free surface.